COMPUTATIONAL NEURAL MODELING AT THE CELLULAR AND NETWORK LEVELS - TWO CASE STUDIES

A Thesis presented to

The Faculty of the Graduate School

University of Missouri – Columbia

In Partial Fulfillment

of the Requirement for the Degree

Masters of Science

By

SANDEEP PENDYAM

Dr. Satish S. Nair, Thesis Supervisor

DECEMBER 2007

The undersigned, appointed by the dean of the Graduate School, have examined the thesis entitled

COMPUTATIONAL NEURAL MODELING AT THE CELLULAR AND NETWORK LEVELS - TWO CASE STUDIES.

presented by Sandeep Pendyam,

a candidate for the degree of Master of Science,

and hereby certify that, in their opinion, it is worthy of acceptance.

Professor Satish S. Nair

Associate Professor Chun S. Lin

Associate Professor Jyotsna Nair

ACKNOWLEDGEMENTS

I would like to express my sincerest thanks to my advisor Dr. Satish Nair for his guidance and support. Without him this work would not have been accomplished. I would like to thank Dr Chun Shin Lin and Dr Jyotsna Nair for being a part of my thesis committee.

I would like to extend my thanks to all of my friends who always are along my side and supported me all through my Master's. Special thanks to my roommates Srikanth, Chaitanya, and Ravi for being special and making my life joyous.

I am also grateful to group members Ashwin, Pavan, Guoshi, Arun, Tai, Tony and Kiran who are always ready to help me in every possible way.

Lastly I would like to thank my mom and my dad for their sacrifices that have made me the person that I am today. I extend my thanks to entire family back in India.

TABLE OF CONTENTS

LIST OF FIGURES

LIST OF TABLES

ABSTRACT

Computational Neuroscience provides tools to abstract and generalize principles of neuronal functions using mathematics, with applicability to the entire neuroscience spectrum. Problems at two levels of the neuroscience spectrum, namely molecular and network are considered in this thesis.

Chapter 1 outlines development of a biologicaly realistic computational model that mimics a junction (synapse) between a single pathway between two different brain regions, prefrontal cortex and nucleus accumbens. This pathway is altered in a chronic cocaine condition. The proposed model which included diffusion of glutamate from the presynapse and it spread through glia into the extracellular space, was then used to provide additional insights into the cellular adaptations due to cocaine. This model proved useful for predicting cocaine-induced changes in a molecular target that was experimentally validated by our collaborating neuroscientist. More generally, this model provided a mathematical framework for describing how pharmacological or pathological conditions influence the synapse. Chapter 2 studies the particular glial configurations of chapter 1 in more detail.

Chapter 3 defines a computational structure to study extinction learning in rats using data from another neuroscience collaborator. The principal structures involved in fear extinction are the amygdala (lateral, basal, intercalated cells, and central nucleus), ventro-medial prefrontal cortex, and the hippocampus. A network model is proposed to study the extinction using artificial neural network models implementing in PDP software.

CHAPTER 1

INTRODUCTION AND OBJECTIVES

1.1. BACKGROUND AND MOTIVATION

Computational neuroscience provides tools to abstract and generalize principles of brain function using mathematics, with applicability to the entire neuroscience spectrum including molecular, cellular, systems, and translational levels (NIH Neuroscience Blueprint 2004). Computational techniques and tools are being developed to model several pathways and brain mechanisms with increasing accuracy and are found to be essential to generate an understanding of the underlying functions in this case (Koch and Segev 2001; Mauk 2000). Indeed, computational models based on the real anatomy and physiology of the nervous system already constitute what is, in effect, a compact and self-correcting database of neurobiological facts and functional relationships (Bower and Bolouri 2001).

The best computational work is both informed by and subsequently contributes to a biological understanding of the nervous system. Computational approaches also allow us to fine tune hypotheses before testing them in biological systems, streamlining the discovery process and decreasing the volume of the use of animal models. Therefore, computational neuroscientists and biological neuroscientists are interdependent groups – neither can reach the full capabilities of their work without the other.

Systems biology aims at system-level understanding of biology in terms of structure, dynamics, control, and design (Hartwell et al. 1999, Kitano 2002) through the integration of all types of biological information at all levels of order and definition of the interactions of individual elements with one another. This integration is eventually formalized as experimentally accessible models that facilitate visualization of the system as a whole. Ideas developed in engineering and computer science such as amplification, adaptation, robustness, insulation, error correction and coincidence detection have been studied in biology for specific systems.

Typically, systems engineers work on dynamical modeling for a wide spectrum of applications ranging from human behavior and weather modeling, to very accurate models for aircraft and automobiles. Interestingly, the process of modeling is the same for all the models in the spectrum, except for the level of complexity and uncertainties involved. Computational models help transition from the 'real world' to the 'math world' where systems from all levels of the spectrum described above look similar. Thus, for systems and control engineers, the techniques of modeling and control are ubiquitous throughout nature, and seem similar. However, control of a system requires that the system be understood 'adequately'. The term 'adequately' implies that the level of understanding of the system is related to the accuracy of control or understanding required. This requirement on control or understanding, typically takes the process of mathematical modeling, for most systems.

1.2 OVERVIEW OF THESIS AND OBJECTIVES

This thesis focuses on the modeling and analysis of certain brain circuits at both molecular (chapters 2 and 3) and network (chapter 4) levels. Each of the chapters 2 – 4 are in the form of stand-alone journal papers, with overall summary provided in chapter 5. The specific objectives of the thesis are listed below under descriptions for chapters 2-4, with the key point being posed as a question in quotes.

Chapter 2 – "what are specific cellular adaptations after chronic cocaine?"

Two important structures involved in the circuit for cocaine abuse and dependence are the nucleus accumbens (NAc) and pre-frontal cortex (PFC) (Kalivas and Volkow, 2005). NAc is part of part of the pleasure system, or reward circuit and is traditionally studied for its role in addiction. The cardinal features of cocaine addiction include uncontrollable urges to obtain drugs and reduced behavioral responding to biological rewards. The fact that these characteristics persist after years of drug abstinence points to enduring neuroplasticity due to cocaine abuse in brain circuitry responsible for processing motivationally relevant stimuli. Augmented responding for drug-associated stimuli and reduced responding for natural rewards arise from cocaine-induced cellular adaptations. Cocaine-induced reduction in cystine-glutamate exchange and mGluR2/3 signaling is shown in Figure 1.1.

The goal is to develop a computational model of elements in the PFC-NAc glutamatergic pathway to study cellular adaptations during withdrawal from cocaine. The overall model for the PFC-NAc pathway functions as follows: the PFC pyramidal cell

fires which results in release of Glu in the PFC-NAc synapse, with the release itself being modulated by a feedback loop involving mGluRs present on the pre-synapse. The Glu released into the synapse diffuses out of the synapse and is largely transported via Glu

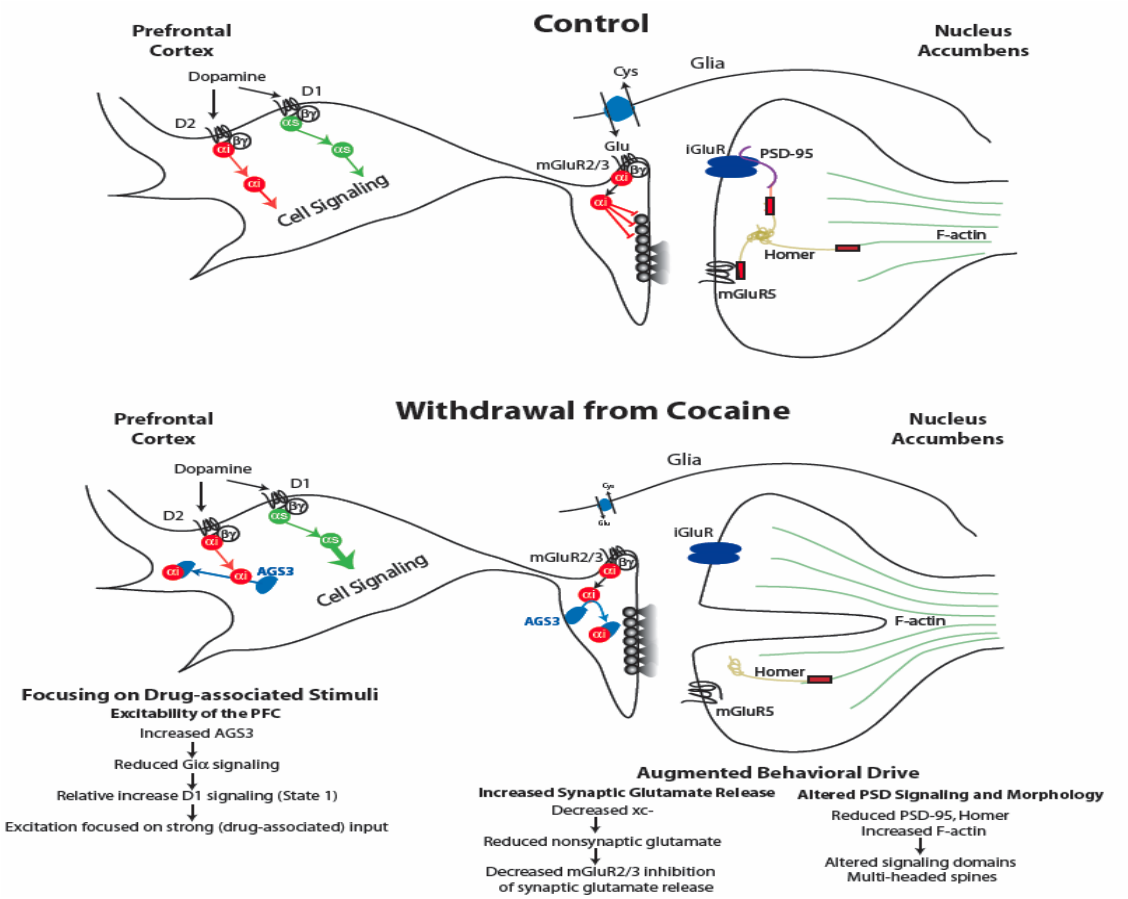

Figure 1.1 Cocaine-induced cellular adaptations in the glutamatergic projections from the prefrontal cortex (PFC) to the nucleus accumbens (NAc) (Kalivas et al. 2005).

transporters on the glial sheath that surrounds the synapse. We have modeled Glu homeostasis in the perisynaptic region considering synaptic Glu release, transporter dynamics, tortuosity, and the CG exchangers, to highlight the importance of the various mechanisms involved.

Chapter 3 – "what are possible glial configurations around a PFC-NAc synapse?"

Synapses are specialized junctions through which the neuronal cells communicate with each other by releasing neurotransmitters such as glutamate. Synapses and their characteristics are being studied by numerous research groups around the world. The perisynaptic region is comprised of glial sheaths that hold glutamate removal proteins called transporters (XAG), and Cystine glutamate (CG) exchangers that produce glutamate. Even with specialized equipment and extensive research, the perisynaptic space (region around the synapse) remains poorly characterized presently. Chapter 3 focused on analyzing possible geometries for glial sheaths that surround a synapse, and characterizing the parameters involved in glutamate homeostasis around a synapse.

Chapter 4 – "what is the regional network involved in fear extinction?"

An artificial neural network model is proposed to study fear extinction. The model will be created using PDP++ software. The network model will be trained and tested and then used in lessoning studies to investigate certain hypotheses regarding the fear circuit functioning, and will also be used to determining resultant characteristics, including specifics of neuroplasticity.

CHAPTER 2

COMPUTATIONAL MODEL OF EXTRACELLULAR GLUTAMATE IN THE NUCLEUS ACCUMBENS PREDICTS NEUROADAPTATIONS BY CHRONIC COCAINE

2.1 ABSTRACT

Chronic cocaine administration causes instability in extracellular glutamate in the nucleus accumbens that is thought to contribute to the vulnerability to relapse. A computational framework was developed to model glutamate in the extracellular space, including synaptic and nonsynaptic glutamate release, glutamate elimination by glutamate transporters and diffusion, and negative feedback on synaptic release via metabotropic glutamate receptors (mGluR2/3). This framework was used to optimize the geometry of the glial sheath surrounding excitatory synapses, and by inserting physiological values, accounted for known stable extracellular, extrasynaptic concentrations of glutamate measured by microdialysis and glutamatergic tone on mGluR2/3. By using experimental values for cocaine-induced reductions in cystine-glutamate exchange and mGluR2/3 signaling, the computational model failed to represent the experimentally observed increase in glutamate that is seen in rats during cocaine-seeking. However, iterative testing of the model demonstrated that deficit was ameliorated if glutamate transport was reduced. This calculated prediction was

experimentally tested and verified by measuring ~60% reduction in glutamate uptake in tissue slices obtained from the core subcompartment of the nucleus accumbens in rats previously trained to self-administer cocaine. Thus, by including extrasynaptic glutamate release mechanisms and empirical measures of the concentration of extracellular glutamate, this model proved useful for predicting cocaine-induced changes in a molecular target (glutamate transporters) that was experimentally validated. More generally, this model provides a mathematical framework for describing how pharmacological or pathological conditions influence glutamate transmission measured by microdialysis.

2.2 INTRODUCTION

Repeated cocaine administration causes enduring changes in glutamate transmission in the nucleus accumbens that may contribute to the vulnerability to relapse (Kalivas et al., 2005). These changes include alterations in synaptic glutamate release (McFarland et al., 2003), dendritic spine morphology (Robinson and Kolb, 2004), nonsynaptic glutamate release (Baker et al., 2003) and group II metabotropic glutamate receptors (mGluR2/3; Xi et al., 2002). The diversity of neuroadaptations has proven difficult to synthesize into a portrait of cocaine-induced pathology. While obtaining experimental measurements of glutamate transmission is critical, an alternate approach is to mathematically model an 'archetypal' synapse by extracting common features of the synaptic environment from a large number of synapses (Clements et al., 1992; Rusakov and Kullmann, 1998; Rusakov, 2001; Barbour, 2001; Diamond, 2005). In the past, these models have focused on synaptic glutamate release, diffusion out of the synapse and

elimination by glutamate transporters (XAG) in an effort to understand the accessibility of synaptically released glutamate to the extracellular environment.

Previously developed mathematical models are based upon electrophysiological research and are appropriate for assessing concentrations of glutamate in the synaptic cleft and the near adjacent perisynaptic environment. However, *in vivo* extrasynaptic concentrations assessed by microdialysis reveal that the majority of glutamate outside of the synaptic cleft is not of synaptic origin (Miele et al., 1996; Timmerman and Westerink, 1997; Melendez et al., 2005). Also, extracellular glutamate in tissue slices and cell culture experiments is partly of nonsynaptic origin (Jabaudon et al., 1999; Haydon, 2001). While a number of sources of nonsynaptic extracellular glutamate have been suggested (Attwell et al., 1993; Danbolt, 2001; Haydon, 2001), extracellular glutamate measured by microdialysis in the nucleus accumbens arises primarily from cystine-glutamate exchange (xc-; Baker et al., 2002; Xi et al., 2002). Cystine-glutamate exchange is the rate-limiting step in glutathione synthesis (McBean, 2002), and glutamate derived from xc- stimulates perisynaptic mGluR2/3, and thereby inhibits synaptic glutamate release (Xi et al., 2002; Moran et al., 2005).

The data above indicate that mathematical modeling of glutamate transmission should include nonsynaptic sources of glutamate. Moreover, rats withdrawn from chronic cocaine administration show dysregulation of extracellular glutamate in the nucleus accumbens due, in part, to reduced xc- and mGluR2/3 signaling (Pierce et al., 1996; Hotsenpiller and Wolf, 2002; Xi et al., 2002; Baker et al., 2003). Therefore, including extrasynaptic glutamate is required to model relevant cocaine-induced neuroplasticity. Also, while mathematical models considering only synaptically released glutamate

predict that each glutamate synapse functions in relative isolation from other synapses (Kleinle et al., 1996; Barbour, 2001; Lehre and Rusakov, 2002; Sykova, 2004), microdialysis during cocaine-seeking measures significant overflow of synaptic glutamate (McFarland et al., 2003, 2004).

In order to predict the cocaine-induced overflow of synaptic glutamate, we modeled synaptic glutamate transmission, different glial geometries populated with XAG and xc-, and the regulation of glutamate release by mGluR2/3. Using physiological values from the literature and empirically derived changes produced by chronic cocaine, the proposed mathematical framework was able to accurately portray both physiological and cocaine altered extracellular glutamate levels.

2.3 METHODS

Model inputs and baseline diffusion, binding and transport parameters

Baseline physiological parameters for glutamate transmission were employed, primarily as described in previous models of glutamate transmission (see Table 2.1). The principal mechanisms involved in transient glutamate dynamics in the perisynaptic region are glutamate diffusion out of the synapse after release, binding to transporters and uptake into glia, production of glutamate by the xc- located in glia (Pow, 2001; Sato et al., 2002), and activation of mGluR2/3 autoreceptors reducing synaptic release probability (Billups et al., 2005; Dietrich et al., 2002; Losonczy et al., 2003).

Synaptic release and regulation by mGluR2/3 autoreceptors:

In vivo estimates of basal firing frequency in prefrontal neurons projecting to the accumbens range from 1 to 3 Hz with the capacity for periods of burst firing up to 15 Hz (Chang et al, 1997; Peters et al., 2005; Sun and Rebec, 2006). Although the probability that an action potential will release a synaptic vesicle ranges from <0.1 to 1 (Allen and Stevens, 1994; Murthy and Sejnowski, 1997), depending upon the experimental preparation the average synaptic release probability more typically ranges from 0.1 to 0.5, with estimates for cortex being at ~0.4 (Trommerhauser et al., 2003; Billups et al., 2005; Volynski et al., 2006). Release probability at glutamatergic synapses is reduced by up to 50% following stimulation of presynaptic mGluR2/3 autoreceptors (Billups et al., 2005; Dietrich et al., 2002; Losonczy et al., 2003), which are located outside of the synaptic cleft (Alagarsamy et al., 2001). Using *in vivo*microdialysis it has been shown that blocking mGluR2/3 elevates extracellular concentrations of glutamate (Xi et al., 2002) and electrophysiological studies in tissue slices reveal that the glutamate providing this tone is derived primarily from nonsynaptic sources (Bandrowski et al., 2003; Moran et al., 2005). In the present mathematical model, basal levels of glutamate in the vicinity of perisynaptic mGluR2/3 were optimized to produce ~50% occupancy, based upon the range of K_d and K_i values reported at this receptor (0.1 to 0.3 μM glutamate; Schoepp and True, 1992). Thus, presynaptic tone on mGluR2/3 was computed in the present model as release probability and was based on linear interpolation over occupancy (max. release probability = 0.4; K_d = 0.187 μM glutamate; slope for control case = 0.32/100, and slope for the cocaine case = 0.1/100). In addition to release probability, each action potential

that resulted in vesicular release was assumed to release 10000 molecules, which is within the range reported by Burns and Jahn (1995) for a wide range of synaptic sizes.

Diffusion:

In a complex medium, several factors can impose constraints on diffusion, including geometry, binding, uptake, viscosity, temperature, or change in structure with time (Nicholson, 2001, Sykova, 2004, Diamond, 2005). Diffusion in the extracellular space is typically characterized by volume fraction α (void space) and tortuosity λ (hindrance to diffusion imposed by local boundaries or local viscosity) (Nicholson, 2001). Estimates of tortuosity λ vary between models since constriction, wiggle and topological factors can problematic (Nicholson, 2001) and the reported range of λ=1.2-2.4 has been based on diffusion measurements over ranges of 100-300 μm (Nicholson, 2001). To account for the viscosity of the medium, interactions with cell walls and extracellular macromolecules our three-dimensional model (Figure 2.1) uses diffusion coefficients in the range of 0.05 to 0.75 μm^2/ms (Rusakov and Kullmann, 1998), and appropriately placed impermeable glial sheaths representing barriers to flow by extracellular structures. Inside the cleft, D_1 (diffusion in free space) was varied from 0.125 to 0.25 μm^2/ms (Savtchenko and Rusakov, 2007); for the free-porous transition (edge of the cleft) diffusion source strength was scaled up by $1/\alpha$ (Rusakov, 2001), and so $D_2 = D_1/\alpha$ with α = 0.12 (Sykova, 2004); D_3 and D_4, which characterize diffusion between the glial sheaths and outside the glial sheaths, respectively, were determined iteratively.

Glutamate transporters (XAG):

Glutamate transport into glia is the primary mechanism for eliminating extracellular glutamate (Danbolt, 2001). The glutamatergic axon terminals from the prefrontal cortex to the accumbens were assumed to be covered by a glial sheath (Lehre et al., 1995). The density of XAG is non-uniform, and glial membranes that face neuropil have a higher expression of transporter than membrane surfaces facing other glia (Cholet et al., 2002). In a model of synaptic release, Rusakov (2001) considered XAG concentration as adjacent to a spherical or semi-spherical glial sheath that surround the neuron. XAG are expressed with a high density in the hippocampus, with surface density ranging from 2500-10,800 molecules/μm^2 (Bergles and Jahr, 1997; Lehre and Danbolt, 1998). Based upon glutamate uptake assays (Colombo, 2005) and transporter binding density (Danbolt, 2001) it was estimated that surface density values for the nucleus accumbens is 22-35% (550-3780 molecules/μm^2) of the value in the hippocampus and cortex. Thus, for the current model the equivalent (assuming glial thickness of 25 nm) surface density of XAG is varied in the range 465-1100 molecules/μm^2 (see Table 2.1), which corresponds to a distribution of 7.7×10^{-22} - 1.81×10^{-21} moles in each glial sheath, which taken together total 8.79×10^{-21} moles. In addition to the concentration of XAG, uptake rates also depend on local glutamate concentration and the kinetic parameters of the transporters (eqn. 3 below).

Cystine-glutamate exchangers (xc-):

The density of xc- and basal rates of cystine-glutamate exchange were estimated as the V_{max} for Glu = 0.5 pmol/μg/min (Murphy et al., 1989; Baker et al., 2003).

Assuming that 1μg protein ≈ 20,000 glial cells (Wang et al., 2005) and that one glial cell equivalent is providing glutamate derived from xc- to a synapse (i.e., 50 pg protein), the estimated basal release of glutamate via xc- in the model was 2.5 x 10^{-17} moles/min, a value within range reported (Wyatt et al., 1996; Warr et al., 1999). Thus, to evaluate various model options, xc- was varied from 8 x 10^{-18} - 25 x 10^{-18} moles/min.

Model inputs and cocaine-induced neuroadaptations

The parameters adjusted in the model to estimate neuroadaptive changes produced by withdrawal from chronic cocaine are outlined in Table 2.2. Withdrawal from daily cocaine administration elicits a 50% reduction in Km for [^{35}S]cystine uptake into accumbens tissue slices (Baker et al., 2003), thereby decreasing the modeled concentration of xc- by 50% (see Table 2.2). Previous studies using [^{35}S]GTPγS binding in accumbens homogenates revealed that G protein coupling to mGluR2/3 is reduced by approximately 70% after cocaine (Xi et al., 2002). Assuming a linear coupling between [^{35}S]GTPγS binding and vesicle release probability, the cocaine-induced reduction in mGluR2/3 function was modeled as release probability increasing from 0.24 to 0.30 in the cocaine treated condition (i.e., a release event occurring every 4.14 action potentials instead of every 3.33 action potentials). Finally, the firing frequency of pyramidal cells in the PFC during cocaine-seeking, a portion of which project to the accumbens, increases from a range of 1-3 Hz to between 10-15 Hz (Sun and Rebec, 2006). Thus, to model activity at the glutamatergic synapse in the accumbens between the basal and cocaine- or food-seeking condition, firing frequency was increased from 1-15 Hz.

Modeling the synapse and glial geometry

Upon release from the synapse (location P_{syn} in fig. 1), glutamate molecules diffuse into the perisynaptic space (Barbour and Hausser, 1997), where glutamate transporter dense astrocytes reduce glutamate spillover to near zero (Diamond and Jahr, 2000; Danbolt 2001). The configuration of the glial sheath (G_i in Figure 2.1) is akin to that previously reported (Rusakov, 2001), but distinct in that in the present model glia are populated with xc-. A thin 25 nm thick spherical layer of free space encloses the edge of the synapse. Glutamate concentration at mGluR2/3 receptors is monitored in the model at the presynaptic location P_{mGluR} in Figure 2.1 ($\theta=20^0$).

Glial membranes were modeled in the form of multiple impermeable sheaths, with free space in between, as an approximation of glial folds. Based upon studies indicating that the highest densities of XAG are perisynaptic (Lehre and Danbolt, 1998; Danbolt, 2001), the XAG-rich region was subdivided into sheaths, region G_1, with a high density of XAG, region G_2, which contains a reduced concentration of XAG, a region G_3 with the lowest density of XAG, and a region G4 with no XAG. Cystine-glutamate exchangers were modeled as being located on the outer surface of the glial membranes of regions G_4 (see Table 2.1). Beyond the glial sheaths, the space contains only glutamate without XAG or xc-. The experimentally defined concentrations of extracellular glutamate reported by *in vivo* microdialysis (Table 2.2) were modeled at point P_{ex} in Figure 2.1, outside glial region G_4.

Mathematical details:

In the configuration of Figure 2.1, the two synaptic hemispheres were assumed rigid permitting no diffusion (i.e., flux = 0 along the periphery), with r = 160 nm from the center, and a separation of δ=20 nm (synaptic cleft) (Rusakov and Kullmann, 1998; Rusakov, 2001; Diamond, 2005). Around this synapse are 40 concentric 25 nm thick shell compartments (i_1- i_{40}) resulting in the outer boundary of the perisynaptic region modeled being at a distance of 1 μm from the edge of the synapse. Each of these shells is divided into 9 compartments (20^o angle increments, j_1-j_9) circumferentially, permitting XAG and xc- concentrations to be assigned individually to each compartment of any shell, as appropriate.

The synaptic cleft volume was discretized into m = (1....N_m) segments where dR_m was the outer radius (R_m=m* dR_m) of the cylindrical elements of thickness δ, each with a volume of $\pi(R_m^2 - R_{m-1}^2)$*δ, with the contact surface between adjacent elements being S_m = $2\pi R_m$*δ. The extracellular space were discretized into i = $(1...N_i)$ concentric spherical elements each of thickness σ, and each spherical element was divided into j = $(1...N_j)$ annular sections where N_j was determined by θ. In the model for the cleft, m=4, and dR_m = 40 nm, and for the spherical shells, σ=25 nm and $\theta = \pi/9$ rad.

The specific mathematical equations used are described next. These are standard conservation and flux equations (see Rusakov (2001) for a comprehensive description including derivations) and have been used to analyze the effect of the proposed glial geometry. A mass balance for extracellular glutamate in each (i,j)th compartment with XAG and xc- yields eqn.1 (Rusakov, 2001),

$$Glu(i,j,t) = Glu(i,j,t-dt) + (J_R \Sigma(i,j,t) S_R + J_T \Sigma(i,j,t) S_T) \frac{dt}{V(i,j)} + (v_+ - v_-)dt \quad (1)$$

where dt is time step, and $S_R(i,j) = 2\pi R_i^2(\cos\theta_j - \cos\theta_{j-1})$ was the surface area between adjacent volume elements in the radial direction, and $S_T(i,j) = 2\pi R_i \sin\theta_j * (\sigma)$ was the surface area shared by adjacent volume elements in the tangential direction, where $R_i = r + \sigma * i$. The radial and tangential fluxes into the compartment were denoted by J_R and J_T, respectively. Each compartment had a volume of $V(i,j) = 0.5(S_R(i,j) + S_R(i-1,j)) * (\sigma)$. The term v_+ accounted for the production of glutamate by xc- and unbinding of glutamate from the transporters ($v_+ = cg(i,j) + k_{-1} * [Glu\text{-}XAG]$, where $cg(i,j)$ is the constant production rate of glutamate by xc- for compartment i,j; see eqn. 3 below), while the term ($v_- = k_1 * [Glu] * [XAG]$) accounted for the reduction in glutamate due to transporter binding. For compartments that are not populated with XAG or xc-, the corresponding terms in eqn. 1 are omitted. Also, eqn.1 is appropriately modified for the compartments in the synaptic cleft, to exclude XAG, xc-, and the tangential flux, and include synaptic release.

The glutamate flux J_{AB} between any two adjacent volume compartments A and B was computed by eqn. 2,

$$J_{AB}(t) = -D\nabla(Glu) = -\frac{D}{ds}(Glu_A(t-dt) - Glu_B(t-dt)) \quad (2)$$

where ds is the spatial distance between compartment centroids and D is the effective diffusion coefficient. For each compartment, this flux was calculated considering two others connected to it radially, and two connected in the tangential direction. Within any

glial compartment, binding of glutamate with transporters is governed by eqn. 3, (Rusakov and Kullmann, 1998),

$$[Glu]+[XAG] \underset{k_{-1}}{\overset{k_1}{\Leftrightarrow}} [Glu-XAG] \overset{k_2}{\Rightarrow} [Glu_{in}]+[XAG] \quad (3)$$

where [*Glu*], [*XAG*], and [*Glu-XAG*] represent the compartmental concentrations of glutamate, transporter, and the bound complex, respectively, and k_2*[Glu_{in}] represents uptake rate of glutamate by XAG.

The discrete form of the differential equation for this kinetic equation is given by eqn. set 4 (Rusakov, 2001):

$$\begin{aligned}
&[Glu]_t = [Glu]_{t-dt} + (-k_1[Glu]_{t-dt}[XAG]_{t-dt} + k_{-1}[Glu-XAG]_{t-dt})dt \\
&[Glu-XAG]_t = [Glu-XAG]_{t-dt} + \{-(k_{-1}+k_2)[Glu-XAG]_{t-dt} + k_1[Glu]_{t-dt}[XAG]_{t-dt}\}dt \\
&[Glu-XAG]_t + [XAG]_t = [Glu-XAG]_{t-dt} + [XAG]_{t-dt} = [XAG_{total}] \\
&[Glu_{in}]_t = [Glu_{in}]_{t-dt} + k_2 * [Glu-XAG]_{t-dt} * dt
\end{aligned} \quad (4)$$

The kinetics for XAG were taken from Rusakov (2001) who based it on experiments by others (Bergles and Jahr, 1998; Wadiche et al., 1995), $k_1 = 10^4\ M^{-1}ms^{-1}$, $k_{-1} = 0.2\ ms^{-1}$, and $k_2 = 0.1\ ms^{-1}$. For all compartments in shell i = 40 (where P_{ex} is measured in Fig. 1), the boundary condition of flux = 0 is imposed at the outer edge, to simulate identical neighboring synapses. That is, no flux enters or leaves the outer boundary of this shell.

Iterative evaluation:

The computational model was developed using C^{++} software (Microsoft Visual Studio, 2005), and an integration time step of 0.5 μs was used. The concentration of glutamate was considered uniform in each compartment and this concentration was updated (eqns. 1-4) at each integration interval based on diffusion, uptake by XAG, and production rates for glutamate, as appropriate. To ensure numerical accuracy, we

performed several tests. The integration time step was decreased by a factor of 10 with no significant change in concentration estimates. At each time step, the numbers of molecules were also computed for free, bound and transported glutamate, to ensure that mass conservation laws were satisfied.

The model in Figure 2.1 (which was also arrived at iteratively; details not shown) was evaluated by changing the following parameters within the ranges outlined in Table 2.1: number of molecules/release, xc- concentration, diffusion coefficients and XAG concentration. The iterative process began using values in the lower end of the range for these parameters and the concentrations of glutamate were monitored at P_{syn}, P_{mGluR}, and P_{ex}, for the basal control case (2 Hz). When the densities of XAG and xc- were iteratively changed, their relative proportions were maintained in the layers of the glial sheath as described above. Through this iterative process, numerous solutions were found that satisfied empirically determined (P_{mGluR}, P_{ex}) or previously calculated (P_{syn}) concentrations of extracellular glutamate for the control case at 2 Hz.

After satisfying the requirements for the basal control case, we simulated the basal cocaine and drug-seeking situation by making known cocaine-induced changes to xc- and mGluR2/3 signaling (modeled as release probability, see above). Through further iterative changes we identified multiple parameter sets that satisfied some of the constraints in Table 2.2, but the model values listed in Table 2.1 constitute the only values that satisfied all the constraints simultaneously.

Animal housing and surgery

Male Sprague-Dawley rats (Harlan, Indianapolis, IN) weighing 250-300 g upon arrival were individually housed in an AALAC-approved animal facility with access to food and water *ad libitum*. Rooms were set on a 12:12-hr light cycle, with lights on at 7:00 A.M and all experimentation was conducted during the light period. All protocols were approved by the Institutional Animal Care and Use Committee in compliance with NIH's Guide for the Care and Use of Laboratory Animals (National Academy Press, Washington D.C., USA, 1996). Prior to surgery the animals were given food and water *ad libitum*. Rats were anesthetized with ketamine HCl (87.5 mg/kg Ketaset, Fort Dodge Animal Health) and xylazine (5 mg/kg Rompum, Bayer), and implanted with indwelling jugular catheters. Threaded guide cannula (C313G, Plastics One, Roanoke, VA) were attached to silastic tubing inserted into the right jugular vein (2.7-3.0 cm) and then was run subcutaneously and externalized on the animals back to attach to an infusion apparatus (McFarland et al., 2003). The catheters were flushed daily with 0.2 ml. of heparin (100 IU/ml) and cefazolin antibiotic (100 mg/ml) in sterile saline vehicle to help protect against infection and maintain patency. After surgery the animals were individually housed for a surgical recovery period of one week. After the recovery period, food was limited to 20 gm/d and water was provided *ad libitum*.

Self-administration and extinction training

Behavioral training began at the end of the seven day surgical recovery period and was conducted as described previously (McFarland et al., 2003). Briefly, after food training, the subjects began cocaine self-administration training. Correct lever presses

resulted in an infusion of cocaine (0.25 mg/kg in 0.05 ml over 3 sec) and also illumination of a stimulus light over the lever. After the 20 sec timeout the light was extinguished, and the first press on the active lever again resulted in cocaine delivery. Sessions lasted for 2 hrs. or until 200 reinforcements were acquired. Rats remained in self-administration training until they met a criterion that the average responding over three consecutive sessions varied by <10%.

During extinction sessions responding on the active lever resulted in illumination of the stimulus light for 20 sec but no infusion of cocaine. Sessions lasted for an hour, followed by a one hour break (in house lights were off and the levers retracted), and then another one hour extinction session. This extinction training protocol continued until subjects met the criterion (<15% of self-administration responding) for three consecutive days.

L-[^{3}H] Glutamate uptake assay:

Rats were decapitated and the prefrontal cortex was rapidly dissected and cut into 350 x 350 μM prism-shaped slices using a McIllwan tissue chopper (Vibratome, St. Louis, MO). The slices were washed for 30 min at 37°C in oxygenated Kreb's-Ringer's solution phosphate buffer (KRP) (in mM: 140 NaCl, 1.3 $CaCl_2$, KH_2PO_4, 5 HEPES, 10 glucose, and 1 $MgCl_2$) with a final pH of 7.4. Glutamate uptake measurements were initiated by adding [^{3}H] glutamate (250 nM, 51 Ci/mmol; PerkinElmer, Boston, MA) in the presence of various concentrations of unlabeled glutamate in a final volume of 250 μL of oxygenated buffer. After incubation at 37°C for 15 min, the uptake was terminated by washing the slices in ice-cold nonradioactive choline-containing buffer. Under these

conditions, [^{3}H]-glutamate uptake was shown to be Na^+-, time-, temperature-, and concentration-dependent (Melendez et al., 2005). Slices were then solubilized using 1% SDS, and the level of radioactivity was determined using a liquid scintillation counter. Protein content in the slices was measured using the Bradford assay. Counts per minute were converted to uptake/mg protein/15 min and treatment groups compared using a two-way ANOVA.

2.4 RESULTS

Geometry of the glial sheath:

Multiple 3-D spherical configurations were studied for glia surrounding the synapse by varying glial coverage, thickness and openings (e.g., see Rusakov, 2001; Barbour, 2001). Table 2.1 shows the range of diffusion coefficients, number of molecules per release, as well as XAG and xc- concentrations in the various glial sheaths (G_1-G_4; see Figure 2.1) that were iteratively varied in order to determine the configuration that brought basal and transient (induced by synaptic release) glutamate concentration in P_{ex} (extracellular compartment sampled by microdialysis) into the range outlined in Table 2.2. Following this iterative process, the configuration in Figure 2.1 proved most robust at sustaining glutamate concentrations within the acceptable ranges. Of note, the value of P_{ex} did not exceed the range measured by microdialysis at firing frequencies of 15 Hz (Table 2.3, Figure 2.2A). Also, by providing resistance to the flow of glutamate this configuration established the necessary gradient to support appropriate levels of extracellular glutamate at P_{syn}, and P_{mGluR}. Thus, at both low and high frequency stimulation P_{mGluR} remained between 0.1 and 0.3 μM, which approximates the K_d for

glutamate binding to mGluR2/3 (Schoepp and True, 1992). Figure 2.2B shows how the increase in P_{mGluR} associated with increased firing frequency negatively regulated release probability. Thus, as P_{mGluR} increased with increased synaptic release of glutamate, the release probability decreased from 0.244 to 0.205. As well, transient glutamate concentrations in the synapse (P_{syn}) were biphasic and within ranges reported by Clements (1996) and Bergles et al. (1999). Thus, as firing frequency ranged from 1 to 15 Hz, the peak concentration in P_{syn} remained near 0.5 mM (Figure 2.2C, 5 ms averages; within 100 μs after release, the concentration falls below 1mM), while the resting concentration between release events ranged from 0.14 to 0.18 μM (Table 2.3)

Effect of withdrawal from chronic cocaine:

Table 2.2 illustrates the alterations made in parameters by incorporating experimentally determined values for reduced xc- and mGluR2/3 desensitization after chronic cocaine (Baker et al., 2003; Xi et al., 2002). In addition, values for Pex approximated the basal values determined by microdialysis in the accumbens that are present after withdrawal from chronic cocaine, as well as peak values elicited after inducing cocaine-seeking after a cocaine injection or stress. The transition from basal and cocaine-seeking behavior is associated with an increase in firing frequency of accumbens neurons, driven in part by inputs from the prefrontal cortex, and firing can range from 1 to 15 Hz (Sun and Rebec, 2006), while the *in vivo* basal firing of prefrontal pyramidal cells is reduced after withdrawal from self-administered cocaine (Trantham et al., 2002; however, see Dong et al., 2005, showing increased excitability of dissociated prefrontal pyramidal cells after chronic cocaine). Therefore, to model this behavioral transition, a

firing frequency range of 1 (basal) to 15 Hz (cocaine-seeking) was employed. The expected value used for basal P_{ex} at 1 Hz was within the range of 2.5-3.4 μM compared with control animals where the concentration of glutamate was expected to be 4.6-6.6 μM (Baker et al., 2003; Szumlinski et al., 2006). When cocaine-seeking was introduced into the model (i.e., 15 Hz firing frequency) P_{ex} was expected to be in the range of 11.9-14.7 μM (McFarland et al., 2003, 2004; Szumlinski et al., 2006). In contrast, in control animals engaging in the seeking of biological rewards (e.g. food), the level of extracellular glutamate at P_{ex} is not expected to differ significantly from basal (i.e. remain in the range of 4.6-6.6 μM; McFarland et al., 2003).

Figures 2.3 and 2.4 illustrate the outcome for P_{syn}, P_{mGluR} and P_{ex} after introducing the cocaine-altered parameters for xc- and mGluR2/3 (modeled as release probability, see Methods) and stimulating synaptic transmission at 1 to 15 Hz. While the model accurately predicted the reduction in basal P_{ex} into the expected range, it did not predict the expected increase in P_{ex} at 15 Hz. Although values after chronic cocaine for both xc- and mGluR2/3 regulation of release probability have been empirically determined, no experimental values for XAG after withdrawal from cocaine have been published. Thus, the model was employed to iteratively explore the effects of changing XAG, and it was found that if XAG was reduced in the range of 50-60%, P_{ex} rose with increasing firing frequency to within the expected range of 11.9-14.7 μM (Figure 2.3). Figure 2.4 shows the data generated using the cocaine parameters including a 60% reduction in XAG. Note that release probability did not change appreciably even though P_{mGluR} increased as a function of increased firing frequency due to the fact that the elevated glutamate levels at

P_{mGluR} exceeded the estimated Vmax of binding to mGluR2 (Schoepp and True, 1992), and that mGluR2/3 signaling is reduced by 70% after chronic cocaine (Xi et al., 2002).

[^{3}H]glutamate uptake:

Based upon the iterations shown in Figure 2.3, the mathematical model predicted that withdrawal from chronic cocaine should reduce XAG in the nucleus accumbens in order to achieve the reported experimental values of P_{ex} reported using microdialysis in cocaine-seeking animals. After 2 wks of extinction training in animals previously trained to self-administer cocaine, tissue slices from the core compartment of the nucleus accumbens were dissected and sodium-dependent [^{3}H]glutamate uptake assayed at three concentrations of glutamate designed to approximate the range previously measured by microdialysis (1, 3 and 5 μM). Figure 2.5 shows that [^{3}H]glutamate uptake was reduced by approximately 60% in tissue slices obtained from rats previously trained to self-administer cocaine versus yoked saline controls.

2.5 DISCUSSION

A computational modeling framework for studying glutamate homeostasis in the prefrontal glutamatergic synapse onto nucleus accumbens spiny cells is reported that accurately predicted extracellular glutamate concentrations as measured by *in vivo*microdialysis (e.g. P_{ex}). The parameters used include those previously employed in computational models of excitatory neurotransmission (see Tables 2.1 and 2.2), such as synaptic release, diffusion from the synaptic cleft and glutamate uptake, as well as parameters not previously modeled, including xc- and negative feedback on synaptic

release by perisynaptic mGluR2/3 (modeled as an effect by extracellular glutamate on synaptic release probability). These latter parameters were included due to a primary goal of this project to model changes in extracellular glutamate concentrations produced by chronic cocaine administration that had been hypothesized to result at least in part from cocaine-induced reductions in xc- and mGluR2/3 signaling (Baker et al., 2003; Xi et al., 2002; Moran et al., 2005). The computational model successfully predicted P_{ex} at low and high firing frequencies in control accumbens. Although accurately predicting the reduction in P_{ex} after chronic cocaine at low firing frequencies, incorporating cocaine-induced reductions in xc- and mGluR2/3 signaling did not predict the large increase in P_{ex} that occurs at the higher firing frequencies achieved during cocaine seeking. To increase P_{ex} during cocaine-seeking, it was necessary to incorporate a reduction in XAG into the model. Importantly, the reduction in XAG predicted by the mathematical model was experimentally verified using sodium-dependent [^{3}H]-glutamate uptake in tissue slices from the nucleus accumbens of animals withdrawn from self-administered cocaine.

Effect of chronic cocaine on glutamatergic transmission

Withdrawal from repeated cocaine administration, whether investigator- or self-administered results in two changes in extracellular glutamate measured by microdialysis, 1) reduced basal concentrations, and 2) increased levels of glutamate after an acute injection of cocaine that induces cocaine-seeking or sensitized motor activity (Pierce et al., 1996; Reid and Berger, 1996; Hotsenpiller et al., 2001; Baker et al., 2003; McFarland et al., 2003). Under basal conditions, glutamate measured by microdialysis is almost entirely of nonsynaptic origin (Miele et al., 1996; Timmerman and Westerink, 1997;

Melendez et al., 2005), while the increase following a cocaine injection in chronic cocaine treated animals is of synaptic origin (i.e. it is blocked by tetrodotoxin or inhibiting prefrontal glutamatergic inputs to the accumbens; Pierce et al., 1996; McFarland et al., 2003). Importantly, an increase in extracellular glutamate (either synaptic or nonsynaptic) does not accompany an acute injection of cocaine or operant responding in animals trained to seek biological rewards such as food (Pierce et al., 1996; Hotsenpillar et al., 2001; McFarland et al., 2003). Thus, in the accumbens of animals chronically pretreated with cocaine, synaptic glutamate transmission appears to escape from the immediate synaptic environment and is measured in significant amounts outside of the synaptic region in P_{ex}. The concentrations of glutamate predicted by the model in P_{mGluR} and P_{syn} are presumably capable of stimulating perisynaptic and synaptic glutamate receptors in adjacent synapses, since at 15 Hz firing frequency (e.g. during drug-seeking), the model predicted that the concentration of glutamate in P_{syn} and P_{mGluR} is 1.7 and 1.9 μM, respectively, and the estimated K_d values for mGluR2/3 and NMDA receptors are in the range of 100-300 nM and 2 μM, respectively (Patneau and Mayer, 1990; Schoepp and True, 1992).

The overflow of synaptic glutamate in animals withdrawn from cocaine is in sharp contrast to the lack of diffusion of significant amounts of synaptic glutamate to adjacent synapses under physiological conditions predicted by previous mathematical models (Barbour, 2001; Lehre and Rusakov, 2002; Sykova, 2004) and experimentally shown using *in vivo* microdialysis (Miele et al., 1996; Timmerman and Westerink, 1997; Melendez et al., 2005). Indeed, even under conditions where animals are behaviorally responding for a natural reward (e.g. food-seeking), there is not significant overflow of

synaptic glutamate measured by microdialysis in the accumbens (McFarland et al., 2003). Therefore, this cocaine-induced overflow constitutes a nonphysiological event that may contribute to the pathology of addiction, as well as contribute to the many neuroplastic changes reported in excitatory synapses in the nucleus accumbens of cocaine treated rats. For example, it has been reported that there is a loss of long-term depression (Martin et al., 2006), an increase in the AMPA/NMDA ratio (Kourrich et al., 2007), an increase in AMPA receptor membrane insertion (Boudreau and Wolf, 2005), an increase in actin cycling and changes in actin regulated proteins in the postsynaptic density (Toda et al., 2006), as well as an increase in dendritic spine density (Robinson and Kolb, 2004). Given the effects of adding glutamate to cultured neurons on dendritic spine formation and postsynaptic density proteins (McGee and Bredt, 2003; Richards et al., 2005), it is possible that the increase in glutamate overflow after cocaine may contribute to the adaptations in excitatory synapses reported after chronic cocaine.

Herein we modeled two cocaine-induced adaptations elicited by chronic cocaine, including reductions in xc- and mGluR2/3 signaling, that were previously proposed to mediate the overflow of synaptic glutamate during drug-seeking, as well as the reduced basal levels. Since xc- is a primary source of extrasynaptically released glutamate (Baker et al., 2002), it was hypothesized that reduced xc- was a major contributor to the reduced basal levels of glutamate (Baker et al., 2003), while reduced negative feedback on synaptic release by down-regulated mGluR2/3 was postulated to promote synaptic release and overflow from the synaptic cleft (Moran et al., 2005). The current mathematical model was designed to incorporate these two parameters in order to evaluate the hypothetical role of xc- and mGluR2/3 neuroadaptations in the cocaine-

induced dysregulation of extracellular glutamate. The mathematical model indicated that considering adaptations in only xc- and mGluR2/3 was inadequate for predicting the increase in synaptic glutamate overflow during drug-seeking (modeled as increased firing frequency of prefrontal afferents to the accumbens). Through iterative calculations with the model, it was shown that reduced XAG could account for the increased overflow during drug-seeking, and the veracity of this prediction was experimentally validated in accumbens tissue slices from rats trained to self-administer cocaine (Figure 2.5).

2.6 Limitations of the proposed mathematical model.

Two general limitations exist in the present attempt to model synaptic and nonsynaptic extracellular glutamate at glutamatergic synapses in the nucleus accumbens. The first limitation is the simplicity of the model relative to the known physiology and cocaine-induced changes in glutamate transmission. Notably, only occupancy of mGluR2/3 is considered in the model, but occupancy of mGluR1 can be expected to change presynaptic release, and this process is altered by chronic cocaine administration (Swanson et al., 2001; Szumlinski et al., 2004). Also, mGluR5 receptor occupancy produces marked changes in synaptic strength due to the induction of long term depression mediated by both post-synaptic and pre-synaptic changes (Malenka and Bear, 2004; Kreitzer and Malenka, 2005). Finally, while the glial geometry used in the framework is a reflection of endogenous tortuosity, it constitutes an oversimplification of the more complicated and varied structural geometry in the extracellular space. In that sense, other configurations with the similar 'resistance' to flow and transporter uptake characteristics might also be feasible. In general, in future models it will be important to

consider more dynamic cellular processes that accompany alterations in firing frequency, as well as more complicated morphological geometries.

The second consideration is that in contrast to the standard mathematical models using postsynaptic currents to empirically validate synaptic concentrations of extracellular glutamate, the present model employed *in vivo* microdialysis measures. Although strengths of microdialysis are that estimates are conducted *in vivo* and nonsynaptic release is readily determined, microdialysis is invasive and will induce damage artifacts distinct from the artifacts associated with in vitro measurements made in a tissue slice. Thus, it has been proposed that the micromolar estimates of extracellular glutamate may result from an artificial accumulation of glutamate in the extracellular space adjacent to the probe (Herman and Jahr, 2007). Indeed, this possibility may have contributed to the glial geometry needed to impose a diffusion barrier between the synapse (P_{syn}) and the site where the dialysis measurements occur (P_{ex}). Regardless of the possible impact of probe-induced damage affecting the concentration of glutamate measured in P_{ex}, it is clear that chronic cocaine administration dramatically alters both basal concentration and the overflow of synaptic glutamate into the extracellular, nonsynaptic environment being sampled by microdialysis, and as shown in the model and empirically, this results in part from down-regulated xc-, XAG and in mGluR2/3 signaling.

2.7 CONCLUSIONS

A computational framework is presented of glutamate transmission that incorporates both synaptic and nonsynaptic glutamate release and homeostatic regulation

of synaptic release via stimulation of mGluR2/3 autoreceptors. This model accurately predicted the basal levels of extracellular glutamate measured by microdialysis, as well as the levels of glutamate in the vicinity of mGluR2/3 that provides inhibitory tone on synaptic release. Also, the model was able to depict the dysregulation of extracellular glutamate accompanying cocaine-seeking, in part by accurately forecasting a down-regulation of XAG. Thus, this model provides a mathematical framework for describing how pharmacological or pathological conditions influence glutamate transmission, and for predicting molecular targets that may be important to experimentally evaluate.

2.8 REFERENCES

Alagarsamy S, Sorensen SD, Conn PJ (2001) Coordinate regulation of metabotropic glutamate receptors. Cur Op Neurobiol 11:357–362.

Allen C, Stevens CF (1994) An evaluation of causes for unreliability of synaptic transmission. Proc Natl Acad Sci 91: 10380-10383.

Attwell D, Barbour B, Szatkowski M (1993) Nonvesicular release of neurotransmitter. Neuron 11: 401-417.

Baker DA, McFarland K, Lake RW, Shen H, Tang XC, Toda S, Kalivas PW (2003) Neuroadaptations in cystine-glutamate exchange underlie cocaine relapse. Nat Neurosci 6:743-9.

Baker DA, Xi ZX, Shen H, Swanson CJ, Kalivas PW (2002) The origin and neuronal function of in vivo nonsynaptic glutamate. J Neurosci 22: 9134-9141.

Bandrowski AE, Huguenard JR, Prince DA (2003) Baseline glutamate levels affect group I and II mGluRs in layer V pyramidal neurons of rat sensorimotor cortex. J Neurophysiol 89:1308-1316.

Barbour B (2001) An evaluation of synapse independence. J Neurosci 21(20): 7969-84.

Barbour B, Hausser M (1997) Intersynaptic diffusion of neurotransmitter. Tr Neurosci 20:377-84.

Bergles DE, Jahr CE (1997) Synaptic activation of glutamate transporters in hippocampal astrocytes. Neuron 19:1297–1308.

Bergles DE, Jahr CE (1998) Glial contribution to glutamate uptake at schaffer collateral-commissural synapses in hippocampus. J Neurosci 18(19):7709-16.

Bergles DE, Diamond JS, Jahr CE (1999) Clearance of glutamate inside the synapse and beyond. Curr Op Neurobiol 9:293–298.

Boudreau AC, Wolf ME (2005) Behavioral sensitization to cocaine is associated with increased AMPA receptor surface expression in the nucleus accumbens. J Neurosci 25:9144-9151.

Billups B, Graham BP, Wong AY, Forsythe ID (2005) Unmasking group III metabotropic glutamate autoreceptor function at excitatory synapses in the rat CNS. J Physiol 565:885-96.

Bruns D, Jahn R (1995) Real-time measurement of transmitter release from single synaptic vesicles. Nature 377: 62-65.

Chang JY, Zhang L, Janak PH,Woodward DJ (1997) Neuronal responses in prefrontal cortex and nucleus accumbens during heroin self-administration in freely moving rats. Brain Res 754: 12–20.

Cholet N, Pellerin L, Magistretti PJ, Hamel E (2002) Similar perisynaptic glial localization for Na+, K+-ATPase alpha 2 subunit and the glutamate transorters GLAST and GLT-1 in the somatosensory cortex. Cereb Cortex 12:515-525.

Clements JD, Robin A, Lester J, Tong G, Jahr CE, Westbrook GL (1992) The time course of glutamate in the synaptic cleft. Science 258:1498-1501.

Clements JD (1996) Transmitter time course in synaptic cleft: its role in central synaptic function. Tr Neurosci 19: 163-171.

Colombo JA (2005) Glutamate uptake by rat brain astroglia incubated in human cerebrospinal fluid. Med Sci Monitor 11:BR13-7.

Danbolt NC (2001) Glutamate uptake. Prog Neurobiol 65:1-105

Diamond JS (2005) Deriving the glutamate clearance time course from transporter currents in CA1 hippocampal astrocytes: transmitter uptake gets faster during development. J Neurosci 25:2906-16.

Diamond JS, Jahr CE (2000) Synaptically released glutamate does not overwhelm transporters on hippocampal astrocytes during high-frequency stimulation. J Neurophysiol 83: 2835-43.

Dietrich D, Kral T, Clusmann H, Friedl M, Schramm J (2002) Presynaptic group II metabotropic glutamate receptors reduce stimulated and spontaneous transmitter release in human dentate gyrus. Neuropharmacology 42:297-305.

Dong Y, Nasif FJ, Tsui JJ, Ju WY, Cooper DC, Hu XT, Malenka RC, White FJ (2005) Cocaine-induced plasticity of intrinsic membrane properties in prefrontal cortex pyramidal neurons: adaptations in potassium currents. J Neurosci 25:936-940.

Haydon P (2001) Glia: listening and talking to the synapse. Nat Neurosci 2:185-191.

Herman MA, Jahr CE(2007) Extracellular glutamate concentration in hippocampal slice. Journal of Neuroscience (2007) 27: 9736-41.

Hotsenpiller G, Giorgetti M, Wolf ME (2001) Alterations in behaviour and glutamate transmission following presentation of stimuli previously associated with cocaine exposure. Eur J Neurosci 14:1843-1855.

Hotsenpiller G, Wolf ME (2002) Extracellular glutamate levels in prefrontal cortex during the expression of associative responses to cocaine related stimuli. Neuropharmacology 43:1218–1229.

Jabaudon D, Shimamoto K, Yasuda-Kamatani Y, Scanziani M, Gahwiler BH, Gerber U (1999) Inhibition of uptake unmasks rapid extracellular turnover of glutamate of nonvesicular origin. Proc Natl Acad Sci 96:8733-8738.

Kalivas PW, Volkow N, Seamans J (2005) Unmanageable motivation in addiction: pathology in prefrontal-accumbens glutamate transmission. Neuron 45:647-50.

Kleinle J, Vogt K, Luscher H -R., Muller R, Senn W, Wyler K, Streit J (1996) Transmitter concentrations profiles in the synaptic cleft: an analytical model of release and diffusion. Biophys J 71:2413-2426.

Kourrich S, Rothwell PE, Klug JR, Thomas MJ (2007) Cocaine experience controls bidirectional synaptic plasticity in the nucleus accumbens. J Neurosci 27:7921-7928.

Kreitzer AC, Malenka RC (2005) Dopamine modulation of state-dependent endocannabinoid release and long-term depression in the striatum. J Neurosci 25: 10537-10545.

Lehre KP, Levy LM, Ottersen OP, Storm-Mathisen J, Danbolt NC (1995) Differential expression of two glial glutamate transporters in the rat brain: quantitative and immunocytochemical observations. J Neurosci 15:1835-53.

Lehre KP, Danbolt NC (1998) The number of glutamate transporter subtype molecules at glutamatergic synapses: chemical and stereological quantification in young adult rat brain. J Neurosci 18:8751-7.

Lehre KP, Rusakov D (2002) Asymmetry of glia near synapse favors presynaptic glutamate escape. Biophys J 83(1):125-134.

Losonczy A, Somogyi P, Nusser Z (2003) Reduction of excitatory postsynaptic responses by persistently active metabotropic glutamate receptors in the hippocampus. J Neurophysiol 89:1910–1919.

Malenka RC, Bear MF (2004) LTP and LTD: an embarrassment of riches. Neuron 44: 5-21.

McBean GJ (2002) Cerebral cystine uptake: a tale of two transporters. Tr Pharmacol Sci 23:299-302

McFarland K, Lapish CC, Kalivas PW (2003) Prefrontal glutamate release into the core of the nucleus accumbens mediates cocaine-induced reinstatement of drug-seeking behavior. J Neurosci 23:3531-3537.

McFarland K, Davidge SB, Lapish CC, Kalivas PW (2004) Limbic and motor circuitry underlying footshock-induced reinstatement of cocaine-seeking behavior. J Neurosci 24:1551-60.

McGee AW, Bredt DS (2003) Assembly and plasticity of glutamatergic postsynaptic assembly. Curr Op Neurobiol 13:111-118.

Melendez RI, Vuthiganon J, Kalivas PW (2005) Regulation of extracellular glutamate in the prefrontal cortex: focus on the cystine glutamate exchanger and group I metabotropic glutamate receptors. J Pharmacol Exp Ther 314:139–147.

Miele M, Boutelle MG, Fillenz M (1996) The source of physiologically stimulated glutamate efflux from the striatum of conscious rats. J Physiol 497:745-751.

Moran MM, McFarland K, Melendez RI, Kalivas PW, Seamans JK (2005) Cystine/Glutamate exchange regulates metabotropic glutamate receptor presynaptic inhibition of excitatory transmission and vulnerability to cocaine seeking. J Neurosci, 25:6389–6393.

Martin M, Chen BT, Hopf FW, Bowers MS, Bonci A (2006) Cocaine self-administration selectively abolishes LTD in the core of the nucleus accumbens. Nat Neuro 9:868-869.

Murphy TH, Miyamoto M, Sastre A, Schnaar RL, Coyle JT (1989) Glutamate toxicity in a neuronal cell line involves inhibition of Cystine transport leading to oxidative stress. Neuron 2:1547-1558.

Murthy VN, Sejnowski TJ (1997) Heterogeneous release properties of visualized individual hippocampal synapses. Neuron 18:599–612.

Nicholson C (2001) Diffusion and related transport mechanism in brain tissue. Rep Prog Physics 64:815-884.

Patneau DK, Mayer ML (1990) Structure-activity relationships for amino acid transmitter candidates acting at N-methyl-D-aspartate and quisqualate receptors. J Neurosci 10:2385-2399.

Peters YM, O'Donnell P, Carelli RM (2005) Prefrontal cortical cell firing during maintenance, extinction, and reinstatement of goal-directed behavior for natural reward. Synapse 56(2):74-83.

Pierce RC, Bell K, Duffy P, Kalivas PW (1996) Repeated cocaine augments excitatory amino acid transmission in the nucleus accumbens only in rats having developed behavioral sensitization. J Neurosci 16(4):1550-l560.

Pow DV (2001) Visualizing the activity of the cystine-glutamate antiporter in glial cells using antibodies to aminoadipic acid, a selectively transported substrate. Glia 34:27-38.

Reid MS, Berger SP (1996) Evidence for sensitization of cocaine-induced nucleus accumbens glutamate release. Neurosci Letts 7:1325-1329.

Richards DA, Mateos JM, Hugel S, De Paola V, Caroni P, Gahwiler BH, McKinney RA (2005) Glutamate induces the rapid formation of spine head protrusions in hippocampal slices. Proc Natl Acad Sci 102:6166-6171.

Robinson TE, Kolb B (2004) Structural plasticity associated with exposure to drugs of abuse. Neuropharmacol 47: 33-46.

Rusakov DA, Kullmann DM (1998) Extrasynaptic glutamate diffusion in the hippocampus: ultrastructural constraints, uptake, and receptor activation. J Neurosci 18:3158-70.

Rusakov DA (2001) The role of perisynaptic glial sheaths in glutamate spillover and extracellular Ca2+ depletion. Biophys J (81):1947-1959.

Sato K, Keino-Masu K, Masu M, Bannai S (2002) Distribution of cystine/glutamate exchange transporter, system xc-, in the mouse brain. J Neurosci 22:8028-8033.

Savtchenko LP, Rusakov DA (2007) The optimal height of the synaptic cleft. Proc Natl Acad Sci 104: 1823-1828.

Schoepp DD, True RA (1992) 1S-3R-ACPD-sensitive (metabotropic) [3H] glutamate receptor binding in membranes. Neurosci Lett 145 (1992):100-104.

Sun W, Rebec GV (2006) Repeated cocaine self-administration alters processing of cocaine-related information in rat prefrontal cortex. J Neurosci 26:8004-8008.

Swanson CJ, Baker DA, Carson D, Worley PF, Kalivas PW (2001) Repeated cocaine administration attenuates group I metabotropic glutamate receptor-mediated glutamate release iand behavioral activation: A potential role for Homer1b/c. J Neurosci 21: 9043-9052.

Sykova E (2004) Extrasynaptic volume transmission and diffusion parameters of the extracellular space. J Neurosci 129:861-876.

Szumlinski KK, Abernathy KE,Oleson EB, Kullmann M, Lominac KD, He DY, Ron D, During M, Kalivas PW (2006) Homer isoforms differentially regulate cocaine-induced neuroplasticity. Neuropsychopharmacology 4:768-77.

Timmerman W, Westerink BH (1997) Brain microdialysis of GABA and glutamate: what does it signify. Synapse 27:242-261.

Trantham H, Szumlinski K, McFarland K, Kalivas PW, Lavin A (2002) Repeated cocaine administration alters the electrophysiological properties of prefrontal cortical neurons. Neuroscience 113: 749-757.

Trommershauser J, Schneggenburger R, Zippelius A, Neher E (2003) Heterogeneous Presynaptic release probabilities: functional relevance for short-term plasticity. Biophys J 84:1563-69.

Volynski KE, Rusakov DA and Kullmann DM (2006) Presynaptic fluctuations and release-independent depression. Nat Neurosci 9:1091-1093.

Wadiche JI, Arriza JL, Amara SG, Kavanaugh MP (1995) Kinetics of a human glutamate transporter. Neuron 14: 1019-27.

Wang Y, Rudnick PA, Evans EL, Li J, Zhuang Z, Devoe DL, Lee CS, Balgley BM. (2005) Proteome analysis of microdissected tumor tissue using a capillary isoelectric focusing-based multidimensional separation platform coupled with ESI-tandem MS. Ann Chem 77(20):6549-56.

Warr O, Takahashi M, Attwell D (1999) Modulation of extracellular glutamate concentration in rat brain slices by cystine-glutamate exchange. J Physiol 514:789-93.

Wolf ME (1998) The Role of amino acids in behavioral sensitization to pychostimulants. Prog Neurobiol 54: 679-720.

Wyatt I, Gyte A, Simpson MG, Widdowson PS, Lock EA (1996) The role of glutathione in L-2-chloropropionic acid induced cerebellar granule cell necrosis in the rat. Arch Tox 70(11):724-35.

Xi ZX, Baker DA, Shen H, Carson DS, Kalivas PW (2002) Group II Metabotropic glutamate receptors modulate extracellular glutamate in the nucleus accumbens. J Pharmacol Exp Ther 300:162–171.

2.9. TABLES

Table 2.1. Ranges for parameter values used in model.

Parameter	**Range of Values (citation)**	**Model Value[a]**
Diffusion coefficient[b] (μm^2/ms)	0.05 – 0.75 (Rusakov and Kullmann, 1998)	see 'b' below
k_1 (M^{-1}ms^{-1})	10^4 (Lehre and Rusakov, 2002)	10^4
k_{-1} (ms^{-1})	0.2 (GLAST/GLT; Lehre and Rusakov, 2002)	0.2
k_2 (ms^{-1})	0.1 (Lehre and Rusakov, 2002)	0.1
No. of molecules per release	4,700 - 80,000 (Bruns and Jahn, 1995)	10000
Intersynaptic distance (μm)	2-20 (Rusakov, 2001)	2
K_d (μM)	0.1-0.3 (Schoepp and True, 1992)	0.187
Maximum release probability	0.1-0.5 (Trommerhauser et al., 2003; Billups et al., 2005; Volynski et al., 2006)	0.4 (max)
XAG conc. (molecules/μm^2)[c]	550-3780 (Bergles and Jahr, 1997; Lehre and Danbolt, 1998; Colombo 2005)	see 'c' below
xc- (moles/min)[d]	8 - 25 x 10^{-18} (Warr et al., 1999)	1.1 x 10^{-17}

[a] Values used to populate model in Figure 2.1 to generate the data shown in Figure 2.2

[b] D_1= 0.125, D_2=D1/0.12 , D_3= D1/0.06, D_4=D_1

[c] surface density (molecules/μm^2) of XAG was distributed as follows: G1a-1094, G1b-1090, G2a-1087, G2b-971, G3a-604, G3b-465, G4a-0, G4b-0

[d] xc^- was distributed uniformly in eight compartments of G4b: (i=12, j = 2-8)

Table 2.2. Parameters altered by chronic cocaine administration.

Parameter	Control	Cocaine	Reference
Glutamate in Pex (μM; basal)	5.6 ± 1.0	2.89 ± .34	Baker et al., 2003; Szumlinski et al., 2006
Peak glutamate in Pex (μM; during food seeking/cocaine-seeking)	5.6 ± 1.0	13.3 ± 1.4	McFarland et al., 2003, 2004.
xc- (moles/min)	1.1 $x10^{-17}$	[a] 4.4 $x10^{-18}$	Baker et al., 2003
Maximum release probability	0.24 (basal) 0.20 (reward)	[b] 0.30	Xi et al., 2002
Firing freq (Hz) (basal)	1-2	1-2	Sun and Rebec, 2006; Trantham et al., 2002
Firing freq (Hz) (drug-seeking)	N/A	3-15	Chang et al., 1997; Sun and Rebec, 2006

[a] Based upon increase in Km for cystine from 2.1±0.2 to 4.2±0.2 μM; 28.3±7.9% reduction in catalytic subunit of xc-

[b] Based upon 70% reduction in mGluR2/3 induced GTPγS binding

Table 2.3 Model predictions at varying firing frequencies using control and chronic cocaine parameters.

Parameters	Control basal	Control biological reward seeking	Cocaine basal[a]	Cocaine drug seeking[a]
Firing freq (Hz)	2	15	1	15
Release probability	0.24	0.20	0.30	0.30
XAG (moles)	8.79×10^{-21}	8.79×10^{-21}	3.51×10^{-21}	3.51×10^{-21}
xc- (moles/min)	1.1×10^{-17}	1.1×10^{-17}	4.4×10^{-18}	4.4×10^{-18}
Estimates of steady state Glu concentrations at three locations				
P_{syn} (μM)	0.143	0.175	0.377	1.73
P_{mGluR} (μM)	0.184	0.226	0.421	1.92
P_{ex} (μM)	5.03	6.08	3.17	12.08

[a] Cocaine-induced reduction in XAG (60%) and mGluR2/3 signaling (70%;modeled as release probability).

2.10. FIGURES

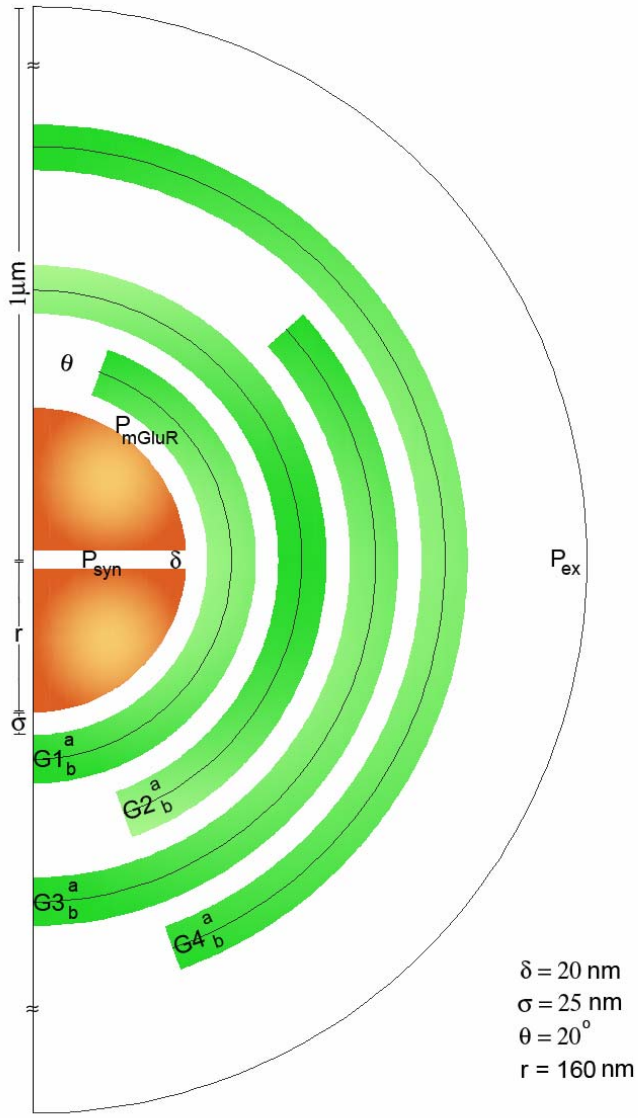

Figure 2.1. Proposed glial configuration to study glutamate homeostasis in the perisynaptic space around the PFC-NAc synapse. Model includes glutamate transporters (XAG) and cystine glutamate exchangers (xc-) in glial regions (green) in varying concentrations to study transients and steady state characteristics. The cleft separates the two hemispheres surrounded by impermeable glial sheaths. The perisynaptic space is partitioned in radial (step σ =25 nM) and tangential (step θ =200) as in Rusakov (2001). Binding, uptake and efflux are computed for each compartment and at its interfaces. Extracellular glutamate was modeled at three sites, within the synaptic cleft (Psyn), at the perisynaptic region containing presynaptic mGluR (PmGluR), and at the site where dialysis probe measures of extracellular glutamate are made (Pex).

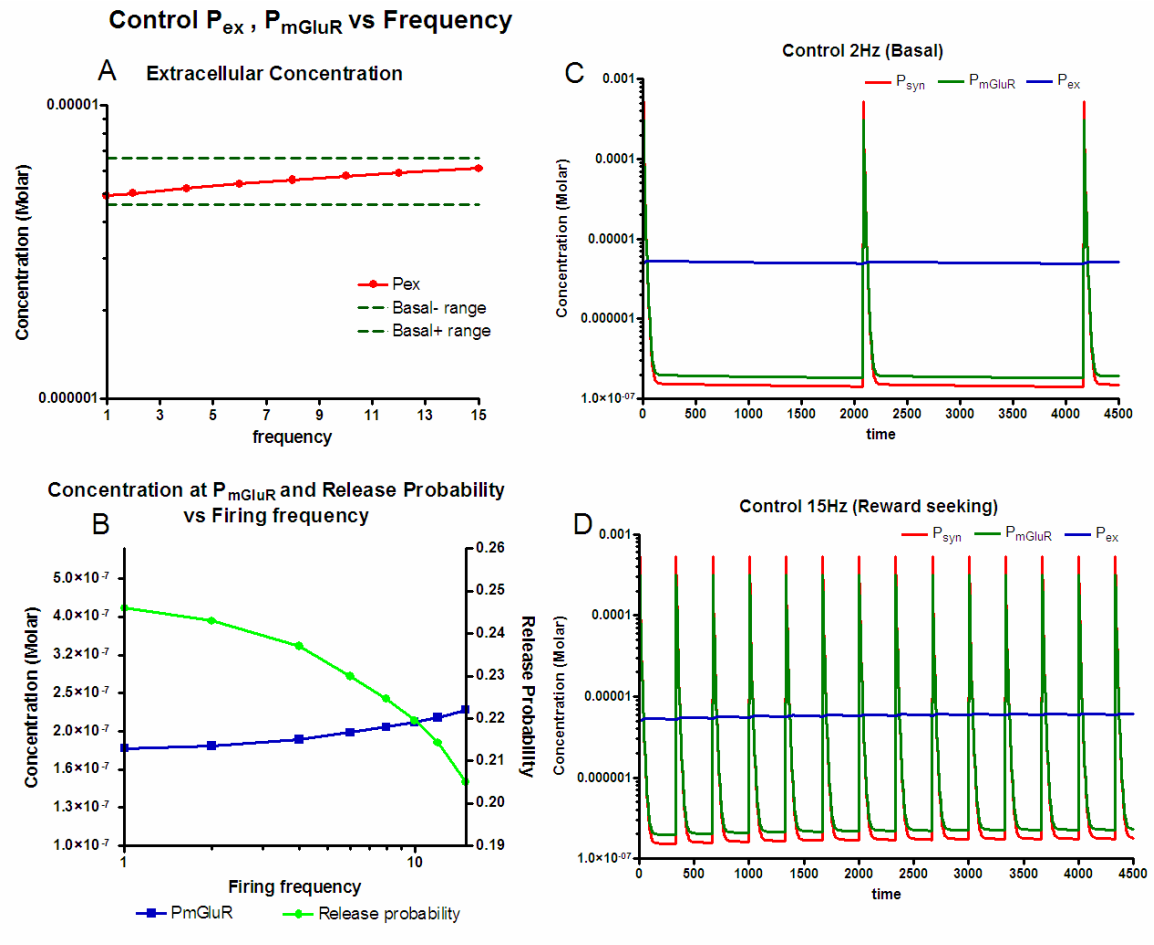

Figure 2.2. Concentrations of glutamate at three spatial locations under control conditions. **A.** The increase in glutamate at Pex remains within the basal range over the full 1-15 Hz range of firing. **B.** As firing frequency increases the concentration of glutamate in the vicinity of perisynaptic mGluR autoreceptors (PmGluR) increases producing a concomitant decrease in release probability. **C.** Model output at 2 and 15 Hz over 4.5 sec, illustrating the dynamic changes in synaptic (Psyn), PmGluR and Pex (e.g. see Figure 1 showing where in the model these measurements were obtained).

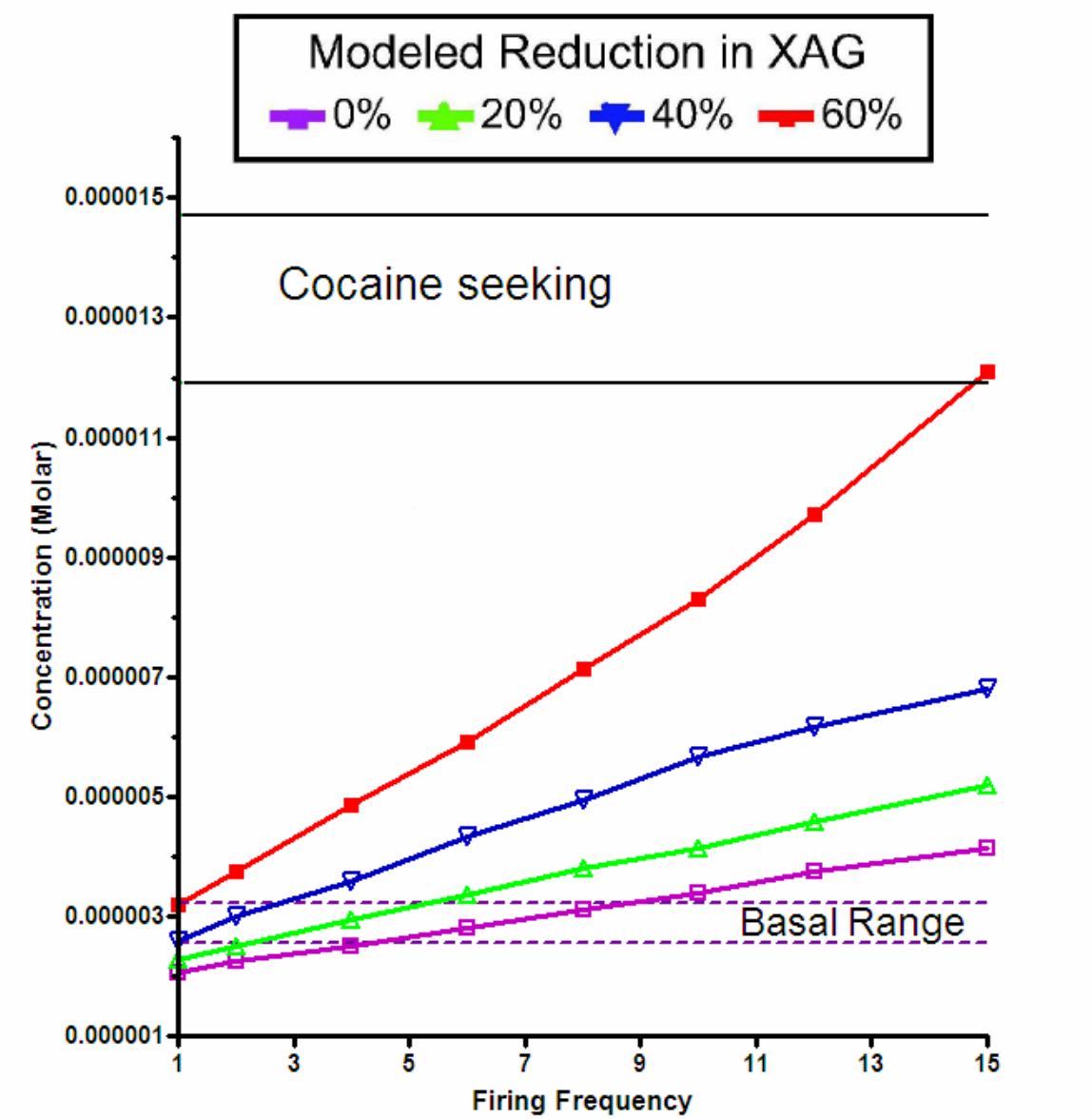

Figure 2.3. Effect of reducing XAG on the concentration of extracellular glutamate in P_{ex}. In cocaine treated rats. To model the cocaine condition, the function of xc- and mGluR2/3 were reduced by 60% and 70%, respectively. Iterations of the model were then run at different concentrations of XAG over a firing frequency range of 1-15 Hz.

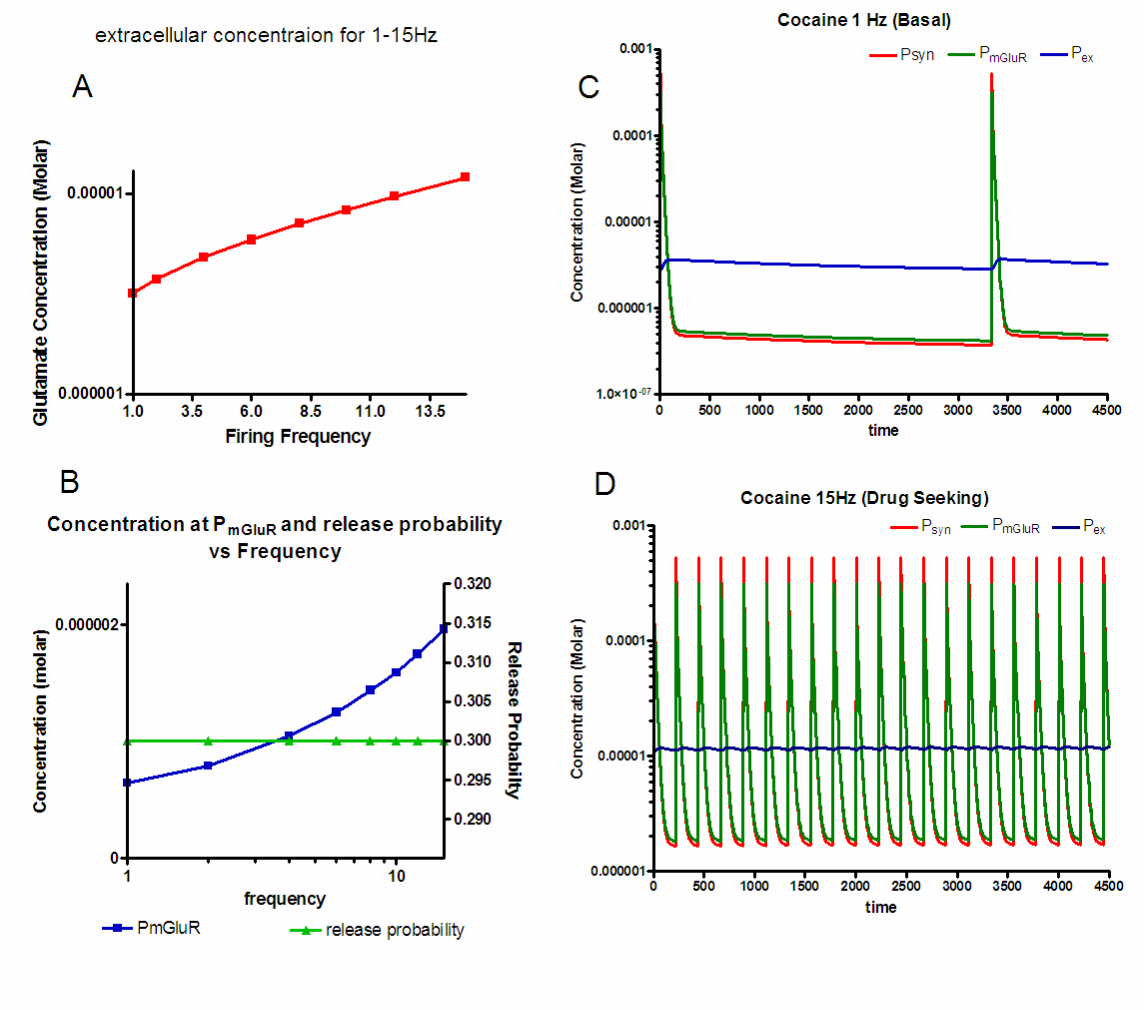

Figure 2.4. Concentrations of glutamate at three spatial locations under cocaine conditions (i.e. xcreduced 60%, mGluR2/3 signaling reduced 70%, XAG reduced 60%). A. The increase in glutamate at Pex is within the basal range at 1 Hz and increases to the cocaine-seeking range at 15Hz firing frequency. B. As firing frequency increases the concentration of glutamate in the vicinity of perisynaptic mGluR autoreceptors (PmGluR) increases without a concomitant decrease in release probability. C. Model output at 1 and 15 Hz over 4.5 sec, illustrating the dynamic changes in synaptic (Psyn), PmGluR and Pex (e.g. see Figure 1 showing where in the model these measurements were obtained).

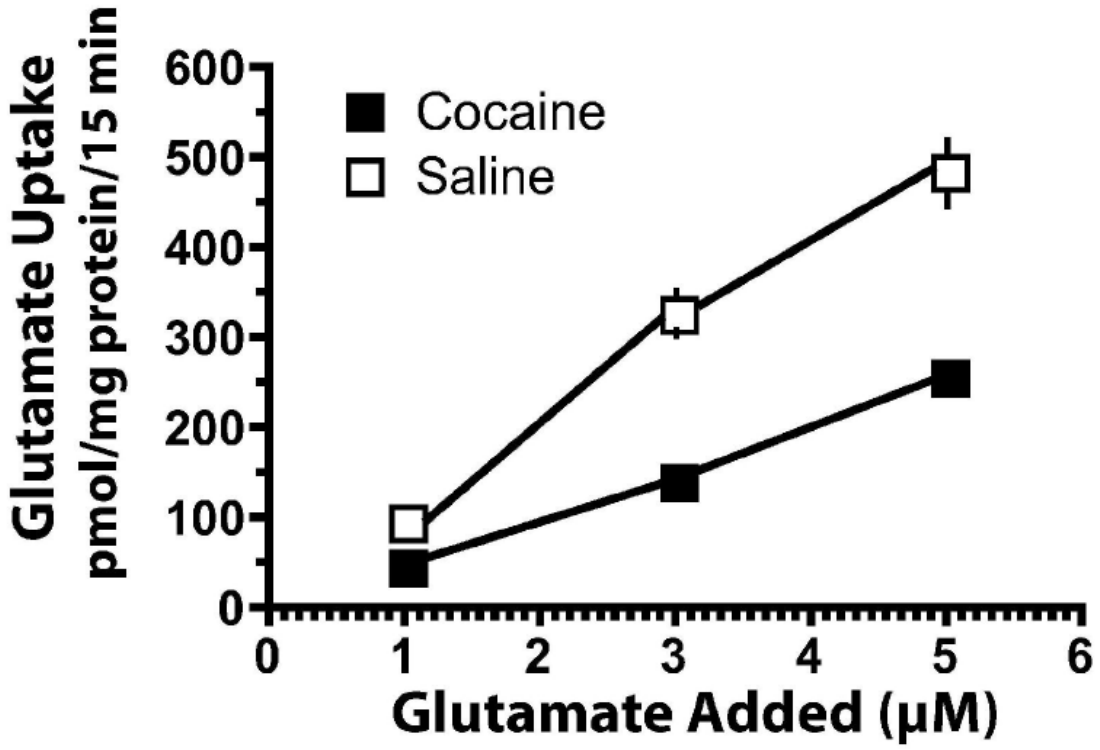

Figure 2.5. [^{3}H]-Glutamate uptake into tissue sliced from the nucleus accumbens core of animals extinguished from cocaine self-administration or yoked saline controls. Data were evaluated using a two-way ANOVA, and significant main effects of treatment (cocaine vs saline; $F(1,26)= 11.36$, $p= 0.002$) and glutamate added ($F(2,26)= 14.73$, $p< 0.001$). No significant interaction between treatment and glutamate concentration was measured. Each data point is shown as mean ± sem of 4-6 determinations run in triplicate.

CHAPTER 3
GLIAL MORPHOLOGY FOR A PFC-NAC GLUTAMATERGIC SYNAPSE

3.1 ABSTRACT

A computational model is developed for a glutamatergic synapse in the prefrontal-accumbal (PFC-NAc) region, by considering the mechanisms involved in glutamate homeostasis. The framework for homeostasis is then used to determine feasible geometries for the glial sheath configurations surrounding the synapse, by matching model estimates with experimental data, using known ranges for parameter values. The framework permits analysis of the role of many distinct glial interactions, and in suggesting possible glial configurations for the synapse.

3.2 INTRODUCTION

Individual synapses can be reconstructed with geometric and environmental details using serial electron micron graphs. However, Rusakov and Lehre (2002) suggest that it would be almost impossible to extrapolate from such studies and draw conclusions about behaviors near an average synapse. The alternative proposed is to extract a few common features from a large number of synapses and reconstruct the environment of an 'archetypal' synapse, representing the synaptic circuitry concerned. Development of such a model requires consideration of possible configurations of the glial structures in the perisynaptic region, in addition to diffusion dynamics and kinetics of the processes. The distribution of transmitter in the synaptic cleft after the release of vesicles depends on a

number of parameters such as the time course of release of transmitter from vesicles, the diffusion coefficient, geometric configuration, binding of transmitters to receptors, and uptake by transporters (Kleinle et al. 1996).

Glial envelopes retain high levels of released neurotransmitter in the synaptic vicinity and the surface rich with transporter molecules take up glutamate from extracellular space (Rusakov 2001). The geometry of extracellular space (ECS) determines how substances diffuse and the activation profiles of the perisynaptic receptors. Geometry appears in the diffusion equations through two dimensionless parameters, volume fraction α and tortuosity λ. Diffusion in the ECS is dependent on and limited by the structure and physio-chemical properties of the ECS.

Diffusion is non homogenous and anisotropic in the ECS. The size and irregular geometry of the diffusion channels substantially differ around individual cells but in different brain regions and thus affect and direct the movement of various neuroactive substances in ECS (Sykova 2004). Tortuosity is a complex parameter incorporating several geometric effects and interstitial viscosity. The "total tortuosity" as measured by ion sensitive microelectrodes measures the slowing of ion movements caused by interactions with macromolecules and membranes. The values for 1.6 for tortuosity and 0.2 for volume fraction have been reported by many regions (Sykova 2004, Nicholson et al 2000).

We integrate several mechanisms and data related to glutamate homeostasis in the PFC-NAc perisynaptic space to develop candidate computational models for glial geometry around a synapse, and then perform parametric studies to characterize them. Previously developed mathematical models are based upon electrophysiological research

and are appropriate for assessing concentrations of glutamate in the synaptic cleft and the near adjacent perisynaptic environment (Clements 1996, Rusakov and Kullmann 1998, Barbour 2001, Rusakov 2001), but do not consider some of the mechanisms included here. The mechanisms considered include glutamate diffusion out of the synapse after release, binding to transporters and uptake in the glial sheath, production of glutamate by the cystine glutamate (CG) exchangers located on the glial sheaths, and activation of mGluR2/3 autoreceptors (Kalivas et al. 2005). Previous research (Pendyam et al., 2008) identified a possible glial configuration and transporter and CG concentrations for a case involving cocaine pathology. Extending that work, we analyze possible glial configurations for a general synapse using two feasible geometries, highlighting its role in glutamate homeostasis.

3.3 METHODS

Perisynaptic geometry

The glutamate projection from the PFC is assumed to be covered by a glial sheath to absorb glutamate overflowing the synapse (Lehre et al. 1995). The geometry of ECS determines how substances diffuse and on the activation profiles of the perisynaptic receptors.

Several configurations for glial coverage with varying concentrations of transporters and CG exchangers are shown in Figure 3.1. The ‘production’ terms for glutamate come from CG exchangers and by vesicular release in the synapse. The glial sheath, with its particular geometry and glutamate transporters act as the ‘control’ to regulate glutamate levels within the perisynaptic space to within physiological limits.

Model dynamics and constraints

The computational model for homeostasis incorporates the mechanisms cited. These mechanisms, parameters and their biophysical ranges are described next. Experimentally reported concentrations of glutamate at certain regions provide other constraints for the model.

Molecules:

The amount of glutamate released at a nerve terminal by exocytosis depends on the size of the synapse, average concentration of glutamate in the vesicles, vesicle volume, vesicles available for exocytosis, diameter of fusion pore and other geometric parameters (Danbolt 2001). Small synaptic contacts are not capable of releasing more than one vesicle of transmitter per presynaptic action potential (Barbour 2001). We considered each action potential that resulted in a vesicular exocytosis was assumed to release 10000 molecules, which is within the range reported by Burns and Jahn (1995) for a wide range of synaptic sizes.

Diffusion:

Diffusion is non-homogenous and anisotropic in the ECS. The size and irregular geometry of the diffusion channels substantially differ around individual cells and thus affect and direct the movement of various neuroactive substances in ECS (Sykova 2004). Diffusion in the extracellular space is characterized by volume fraction α (void space, 0.12-0.22) and tortuosity λ (hindrance to diffusion imposed by local boundaries or local viscosity, 1.4-2.2) (Nicholson, 2001, Sykova 2004). Some previous attempts to model

extrasynaptic glutamate diffusion have relied on simplified geometric representations which are difficult to relate to the neuropil "in vivo" while others incorporated the synaptic cleft surrounded by an isotropic porous medium, described only by extracellular volume fraction and tortuosity factor (Rusakov and Kullmann 1998, Barbour 2001). To account for the viscosity of the medium, interactions with cell walls and extracellular macromolecules our three-dimensional models (Figure 3.1) we use diffusion coefficients in the range of 0.01 to 0.20 $\mu m^2/ms$ within the range reported (Table 3.1; Rusakov and Kullmann 1998, Savtchenko and Rusakov 2007), and appropriately placed impermeable glial sheaths representing barriers to flow by extracellular structures.

Transporters:

High levels of extracellular glutamate are harmful, and removal of extracellular glutamate by Excitatory Amino Acid Transporters (EAAT) is critical to prevent glutamate toxicity (Danbolt 2001). EAATs (which include both GLAST and GLT, though GLT is prominent) are expressed with a high density in the hippocampus, with surface density 2500-11000/μm^2 (Bergles and Jahr 1997, Lehre and Danbolt 1998). The density of GLT transporters is nonuniform, and glial membranes that face neuropil have a higher expression of GLT than membrane surface facing other glia. Based upon glutamate uptake assays (Colombo, 2005) and transporter binding density (Danbolt, 2001) it was estimated that surface density values for the nucleus accumbens is 22-35% (550-3780 molecules/μm^2) of the value in the hippocampus and cortex. Thus, for the models considered, the equivalent (assuming glial thickness of 25 nm) surface density of transporters is varied in the range 456 -8650 molecules/μm^2.

Cystine glutamate exchangers(CG):

Cystine-glutamate exchange is the rate-limiting step in glutathione synthesis (McBean, 2002), and glutamate derived from CG stimulates perisynaptic mGluR2/3, and thereby inhibits synaptic glutamate release (Xi et al., 2002; Moran et al., 2005).

In vivo extrasynaptic concentrations assessed by microdialysis reveal that the majority of glutamate outside of the synaptic cleft is not of synaptic origin (Miele et al., 1996; Timmerman and Westerink, 1997; Melendez et al., 2005). Also, extracellular glutamate in tissue slices and cell culture experiments is partly of nonsynaptic origin (Jabaudon et al., 1999; Haydon, 2001), measured by microdialysis in the nucleus accumbens arises primarily from cystine-glutamate exchange (CG; Baker et al., 2002; Xi et al., 2002). To evaluate various model options, CG was varied from $1.1 \times 10^{-17} – 4.3 \times 10^{-17}$ moles/min.

Metabotropic glutamate receptor occupancy and release probability:

Metabotropic glutamate receptors (mGluR2/3) located presynaptically on glutamatergic nerve terminals modulate the release of the transmitter. Escaping Glu was found to bind more to metabotropic receptors on the pre-synapse as opposed to those on the post-synapse (Baude et al. 1993). Using *in vivo* microdialysis it has been shown that blocking mGluR2/3 elevates extracellular concentrations of glutamate (Xi et al., 2002). Based on the localization of the glial transporters, glutamate transient characteristics and time course, the amount of glutamate available to mGluR2/3 varies the release probability. Although the probability that an action potential will release a synaptic vesicle ranges from <0.1 to 1 (Allen and Stevens, 1994; Murthy and Sejnowski, 1997),

depending upon the experimental preparation the average synaptic release probability more typically ranges from 0.1 to 0.5, with estimates for cortex being at ~0.4 (Trommerhauser et al., 2003; Billups et al., 2005; Volynski et al., 2006).

Model development

Modeling glial geometry. The molecules are released at the centre of the synaptic cleft and the molecules diffuse out through the cleft into perisynaptic area. Upon release from the synapse, glutamate molecules diffuse into the perisynaptic space (Barbour and Hausser 1997), where glutamate transporter dense glial astrocytes reduce glutamate spillover and repackage glutamate for subsequent release (Danbolt 2001). The mGluR2/3 are part of the negative feedback loop to control Glu release from the PFC terminals. The transporter rich region is modeled and subdivided into multiple impermeable sheets as an approximation of glial folds, with a region high density of transporters, a region with reduced concentration of transporters, and a region with the lowest density of transporters(depending on configuration). Cystine-glutamate exchangers are modeled as being located on the outer surface of the glial membrane of regions.

In the configuration of Figure 3.1, the two synaptic hemispheres were assumed rigid permitting no diffusion (i.e., flux = 0 along the periphery), with r = 160 nm from the center, and a separation of δ=20 nm (synaptic cleft) (Rusakov and Kullmann, 1998; Rusakov, 2001; Diamond, 2005). Around this synapse are 40 concentric 25 nm thick shell compartments (i_1- i_{40}) resulting in the outer boundary of the perisynaptic region modeled being at a distance of 1 μm from the edge of the synapse. Each of these shells is divided into 9 compartments (20^o angle increments, j_1-j_9) circumferentially, permitting

transporters and CG concentrations to be assigned individually to each compartment of any shell, as appropriate.

The synaptic cleft volume was discretized into $m = (1....N_m)$ segments where dR_m was the outer radius ($R_m = m * dR_m$) of the cylindrical elements of thickness δ, each with a volume of $\pi(R_m^2 - R_{m-1}^2)*\delta$, with the contact surface between adjacent elements being $S_m = 2\pi R_m*\delta$. The extracellular space were discretized into $i = (1...N_i)$ concentric spherical elements each of thickness σ, and each spherical element was divided into $j = (1...N_j)$ annular sections where N_j was determined by θ. In the model for the cleft, m=4, and dR_m = 40 nm, and for the spherical shells, σ=25 nm and $\theta = \pi/9$ rad.

The specific mathematical equations used are described next. These are standard conservation and flux equations (see Rusakov (2001) for a comprehensive description including derivations) and have been used to analyze the effect of the proposed glial geometry. A mass balance for extracellular glutamate in each $(i,j)^{th}$ compartment with transporters and CG yields eqn.1 (Rusakov, 2001),

$$Glu(i,j,t) = Glu(i,j,t-dt) + (J_R \Sigma(i,j,t) S_R + J_T \Sigma(i,j,t) S_T) \frac{dt}{V(i,j)} + (v_+ - v_-)dt \qquad (1)$$

where dt is time step, and $S_R(i,j) = 2\pi R_i^2(\cos\theta_j - \cos\theta_{j-1})$ was the surface area between adjacent volume elements in the radial direction, and $S_T(i,j) = 2\pi R_i \sin\theta_j * (\sigma)$ was the surface area shared by adjacent volume elements in the tangential direction, where $R_i = r + \sigma * i$. The radial and tangential fluxes into the compartment were denoted by J_R and J_T, respectively. Each compartment had a volume of $V(i,j) = 0.5(S_R(i,j) + S_R(i-1,j)) * (\sigma)$. The term v_+ accounted for the production of glutamate by CG and unbinding of glutamate from the transporters ($v_+ = cg(i,j) + k_{-1} * [Glu\text{-}T]$, where $cg(i,j)$ is the constant production

rate of glutamate by CG for compartment i,j; see eqn. 3 below), while the term (v_{-} $=k_1$*[Glu]*[T]) accounted for the reduction in glutamate due to transporter binding. For compartments that are not populated with transporters or CG, the corresponding terms in eqn. 1 are omitted. Also, eqn.1 is appropriately modified for the compartments in the synaptic cleft, to exclude transporters, CG, and the tangential flux, and include synaptic release.

The glutamate flux J_{AB} between any two adjacent volume compartments A and B was computed by eqn. 2,

$$J_{AB}(t) = -D\nabla(Glu) = -\frac{D}{ds}(Glu_A(t-dt) - Glu_B(t-dt)) \qquad (2)$$

where ds is the spatial distance between compartment centroids and D is the effective diffusion coefficient. For each compartment, this flux was calculated considering two others connected to it radially, and two connected in the tangential direction. Within any glial compartment, binding of glutamate with transporters is governed by eqn. 3, (Rusakov and Kullmann, 1998),

$$[Glu] + [XAG] \underset{k_{-1}}{\overset{k_1}{\Leftrightarrow}} [Glu - XAG] \overset{k_2}{\Rightarrow} [Glu_{in}] + [XAG] \qquad (3)$$

where [Glu], [T], and [Glu-T] represent the compartmental concentrations of glutamate, transporter, and the bound complex, respectively, and k_2*[Glu_{in}] represents uptake rate of glutamate by transporters.

The discrete form of the differential equation for this kinetic equation is given by eqn. set 4 (Rusakov, 2001):

$$
\begin{aligned}
[Glu]_t &= [Glu]_{t-dt} + (-k_1[Glu]_{t-dt}[T]_{t-dt} + k_{-1}[Glu-T]_{t-dt})dt \\
[Glu-T]_t &= [Glu-T]_{t-dt} + \{-(k_{-1}+k_2)[Glu-T]_{t-dt} + k_1[Glu]_{t-dt}[T]_{t-dt}\}dt \\
[Glu-T]_t &+ [T]_t = [Glu-T]_{t-dt} + [T]_{t-dt} = [T_{total}] \\
[Glu_{in}]_t &= [Glu_{in}]_{t-dt} + k_2 * [Glu-T]_{t-dt} * dt
\end{aligned}
\qquad (4)
$$

The kinetics for transporters were taken from Rusakov (2001) who based it on experiments by others (Bergles and Jahr, 1998; Wadiche et al., 1995), $k_1 = 10^4\ M^{-1}ms^{-1}$, $k_{-1} = 0.2\ ms^{-1}$, and $k_2 = 0.1\ ms^{-1}$. For all compartments in shell $i = 40$ (where P_{ex} is measured in Figure. 3.1), the boundary condition of flux = 0 is imposed at the outer edge, to simulate identical neighboring synapses. That is, no flux enters or leaves the outer boundary of this shell.

Determining feasible solution:

The computational model is developed using C^{++} software, and an integration time step of 0.5 μs. The iterative process began using values in the lower end of the range for these parameters and the concentrations of glutamate were monitored at P_{syn}, P_{mGluR}, and P_{ex}, for the basal control case (2 Hz). For instance, for this case we found that the concentration at P_{syn} and P_{mGluR} were very high, and to reduce them, transporter density was altered, maintaining a higher proportion near the synapse. With increase in transporter density the extracellular concentration decreases, and to compensate for this reduction we increase CG density. Changing the diffusion coefficient would cause a change in these concentrations with P_{syn}, P_{mGluR} changing in a direction opposite to this change, and P_{ex} changing in the same direction. The densities of transporters and CG were iteratively changed to get this case working. The number of molecules/release was still in the low range and was not important, i.e., the constraints could be satisfied with any number of molecules/release. We thus find numerous solutions that satisfy the

control case for 2 Hz. After this, we check for the reward seeking ('Control 12 Hz case') condition, and found that the extracellular concentration was within bounds. The number of molecules/release affects this case and we found that 10,000 molecules/release was the maximum permissible to satisfy this condition.

In this process of determining model parameters we found multiple sets that satisfied some of the constraints, but the proposed configuration 2 was the only one that satisfied all the constraints simultaneously. The robustness of the parameter set for this configuration is studied in more detail later.

3.4 RESULTS AND DISCUSSION

Steady state and transient dynamics

Configuration1: A systematic study of electron micrographs from the vicinity of common cerebellar and hippocampal synapses (Rusakov and Lehre, 2002) reveal that the glial processes have direct contact with the synapse, and are higher on the post-synaptic side since they are found to be 2-4 times likely to activate presynaptic receptors. This motivates the proposed configuration 1 where the glial sheaths are in direct contact with the synapse on the post-synaptic side (Rusakov 2001, Fig 1A) and are impermeable, thus taking into consideration both the findings just cited. The sheaths G_1 and G_2 populated with transporters are present in compartments j_2 to j_9 of layers i_2-i_3 and i_5-i_6 as shown in Fig 1A. CG was populated in the other surface compartments j_2 to j_9 of layer i_6 in G_2.

Configuration2: Based on the concentration estimates using configuration 1, a modified configuration, configuration 2 (Fig.1) is proposed which results in a longer path for the glutamate molecule, and simultaneously permits the following: (i) similar uptake

rates with fewer transporters, by reducing transporter saturation, and (ii) reduced effect of extracellular glutamate (in the outer shells) on the synaptic concentration by forcing a Glu gradient. Glial membranes were modeled in the form of multiple impermeable sheaths, with free space in between, as an approximation of glial folds. Based upon studies indicating that the highest densities of transporters are perisynaptic (Lehre and Danbolt, 1998; Danbolt, 2001), the transporter-rich region was subdivided into sheaths, region G_1, with a high density of transporters, region G_2, which contains a reduced concentration of transporters, a region G_3 with the lowest density of transporters, and a region G4 with no transporters. Cystine-glutamate exchangers were modeled as being located on the outer surface of the glial membranes of regions G_4 (see Table 3.1). Beyond the glial sheaths, the space contains only glutamate without transporters or CG. The experimentally defined concentrations of extracellular glutamate reported by *in vivo* microdialysis (Table 3.2) were modeled at point P_{ex} in Figure 3.1, outside glial region G_4.

The geometry in configuration 2 was able to satisfy the constraints much better as seen from the estimates in Table 3.2. The concentration near synapse P_{syn} was ~100 nM, concentration at P_{mGluR} was 184 nM, close to the k_d value of 187 nM. The model has different diffusion coefficients in various regions of the perisynaptic space to conform to reported transient (Clements et al. 1992) and steady state (Baker et al 2003, Danbolt 2001) Glu time courses. Synaptic diffusion was assumed to be 0.125 μm^2/ms in the cleft with an increased value of $0.125/\alpha$ μm^2/ms at the edge where α=0.12 and diffusion in glia of D3=0.06 μm^2/ms. A value of D=0.06 μm^2/ms was used past the edge of the synapse, i.e., through the glial structures. Outside the glial structure free space region, a value of D=0.125 μm^2/ms was used. A combination of these diffusion coefficients, and

appropriate transporter and CG concentrations selected (Table 3.3), successfully predicted transient (Clements et al. 1992) and steady state experimental data for glutamate time courses for the cases considered. The glial structure provides an extended path for molecules and acts as 'valve' that regulates the inflow.

Comparison:

Concentration estimates from configuration 1 show that it is incapable of sustaining a gradient from P_{ex} of 5 μM in the extracellular space to 100nM near the synapse. The transporter density was maintained at a constant value of 3850 molecules/μm^2, the maximum density observed in nucleus accumbens (Colombo, 2005 and Danbolt, 2001). The CG exchanger density was adjusted to achieve 5 μM at P_{ex}. With this parameter set one would expect maximum uptake. However, varying diffusion changes the concentration in P_{syn}, P_{mGluR} , and P_{ex}. With a diffusion coefficient of 0.05 μm^2/ms, the concentrations at P_{syn}, P_{mGluR} , and P_{ex} are 650nM, 1.25 μM and 4.95 μM respectively. For this, very high transporter density and very low diffusion coefficient is required in regions apposite to synapse. For the case considered, we find that 650 nM will be the least concentration that can be achieved with configuration 1, if an extracellular concentration of 5 μM is used. Hence, configuration 1 could be characterized as being capable of sustaining a concentration at P_{syn} of only 10-15% of the concentration at P_{ex}. For configuration 2, however, concentrations at P_{syn}, P_{mGluR} , and P_{ex} of 84 nM, 150 nM and 5.15 μM, respectively, were achieved with less rigorous constraints on the parameters (Table 3.3), due to a more 'efficient' geometry. Configuration 2 can be characterized as being capable of sustaining concentrations at P_{syn} of upto 1.5 % of the

concentration at P_{ex}. Figure 3.2 also shows that the gradient in configuration 1 is rather abrupt, as compared to the gradual one for configuration 2.

Transient analysis

Following a synaptic release, the glutamate time course in the cleft depends on the number of molecules/release, the geometry and its diffusion characteristics. In the iterative optimization process, both steady state (just cited) and transient characteristics are optimized simultaneously. Estimates of time course for Glu clearance from the synapse have been provided by Clements et al (1992) as follows: a) Glu concentration cannot be greater than 1mM in the cleft for more than 100-200μs to prevent the alteration neuronal excitability by desensitizing the receptors. The transient characteristics of the proposed model satisfied this requirement with the Glu concentration at the center of the cleft was found to be more than 1mM for 187 μs matching closely the trend reported by Clements et al. (1992). The plots for the case with and without CG exchangers coincide, they exactly overlap this shows cg exchangers or extracellular glutamate have no effect on the transient dynamics in the synaptic cleft.

The average concentration of transmitter in the cleft ranges 1-5 mM and its clearance from the cleft is biphasic (Clements 1996). In the first phase glutamate is distributed evenly throughout the synapse in 50-200 μs (τ_1), and in the second phase which lasts 0.5-5 ms (τ_2), depending on synaptic geometry, glutamate molecules escape into the extracellular space. From a curve fit of the transient response for configuration 2, the decay in synaptic concentration was found to be biphasic with the following equation: $[Glu(t)] = (0.0001) + (0.000628) \exp^{(-21.706t)} + (0.000628) \exp^{(-0.29785t)}$.

Comparing this with the biphasic characteristic $Y_o + A_1\exp(-t/\tau_1) + A_2\exp(-t/\tau_2)$, we get $\tau_1 = 56.7$ μs and $\tau_2 = 3.35$ ms. This shows that configuration 2 satisfies the transient characteristics reported in Clements (1996).

Robustness and Sensitivity analysis

The two configurations are further characterized by considering the robustness of their estimates as the key parameters varied. The key parameters were first determined and the robustness study was performed by comparing estimates for concentrations as the following parameters are varied ±10% from their optimal values: XAG density, D3, molecules/release, release probability, and the gap between glial folds. The findings are summarized in Table 3.3.

Transporter Density (XAG):

If the total transporters in the system are increased by 10% then the concentrations at P_{ex}, P_{mGluR} and P_{syn} decreases by 20-22%, 18-20% and 4-6%, respectively, for configuration 2 and 8-10%, 9-11% and 8-11% for configuration 1. If the total transporters are decreased by 10% P_{ex}, P_{mGluR} and P_{syn} is found to increase in a similar fashion. From modeling perspective if a change in concentration in all three regions is required, then the total number of transporters in the system will need to be changed.

Diffusion coefficient in glia (D3)

If the diffusion coefficient D3 in the glia is increased by 10% in configuration 2, an increase is observed in Glu concentration at P_{syn} and P_{mglur} by 13 % and 10%,

respectively, but it decreases at P_{ex} by 4.4%. If D3 is decreased by 10%, P_{syn} and P_{mglur} decrease by 15% and 12%, respectively, while P_{ex} increases by 4.9%. In configuration 1 for an increase in D3 by 10%, an increase in P_{syn} and P_{mglur} by 2.5 % and 10%, respectively and a decrease of 2% in P_{ex} was observed. Decreasing D3 in configuration 1 we observe an decrease in P_{syn} and P_{mglur} by 2.5 % and 10%, respectively and an increase of 2% at P_{ex} . So, D3 can be adjusted if concentration near synapse (P_{ex} & P_{mGluR}) needs to be increased, and P_{ex} decreased, or vice versa.

Molecules per release and release probability:

These release parameters are not effective at lower frequencies and thus, does not impact concentrations significantly. But, at higher frequencies a subsequent release can occurs before the system attains steady state from a previous release. During reward seeking situation peak firing frequencies can be around 15 Hz. In such situation (higher frequencies) an increase in number of molecules per release by ±10% would increase the concentration Pex, P_{mGluR} and P_{syn} by ±14-16% in configuration 2. During reward seeking (15 Hz) case in configuration2 changing release probability by 10% increased concentration at Pex, P_{mGluR} and P_{syn} by 1.2%, 3% and 7% respectively. There was no change in concentration when the number of molecules per release, or release probability was increased or decreased by 10% in configuration1. This effect is due to very high concentration of transporters populated in configuration1.

Varying the extracellular gap

With the synaptic dimensions held constant we changed the extracellular gap and studied the effects of varying this parameter for configuration 2. Thorne and Nicholson

(2006) reported an extracellular space between 38-64 nm while modeling fluid-filled pores. When the gap between glial folds of 75 nm (i.e. free space 25nm and transporter space 50nm) is decreased to 60 nm (i.e., free space 20 nm and transporter space 40 nm), extracellular concentration was at 4.2 μM , synaptic at 120 nM and near mGluR it was 220 nM. The total transporter concentration had to be decreased by 15% to obtain an extracellular concentration of 5μM. The diffusion coefficient also had to be decreased from 0.06μm^2/ms to 0.05 μm^2/ms, to decrease the concentration at P_{syn} and P_{mGluR}. When shell size is increased, an increase in transporters concentration is needed to maintain the extracellular concentration at 5 μM. An increase in transporters is required, since changing the shell size increases the volume and to compensate for transporter density, concentration has to be increased. As shell thickness is changed, glutamate concentration decreases near P_{syn} and P_{mGluR} to 90 nM and 120 nM, respectively. Increasing diffusion will increase P_{syn} and PmGluR during steady state, as a higher diffusion coefficient ensures lower uptake. We had to increase the diffusion coefficient from 0.06 μm^2/ms to 0.07 μm^2/ms, to increase the concentration at P_{syn} and P_{mGluR}.

The sensitivity list for the parameters for (1) control basal '2Hz' case & (2) control reward seeking '15 Hz' case with different parameters such as transporter density (XAG), diffusion in glia (D3) and number of molecules/release (molecules) is:

Control basal '2 Hz' case: P_{ex} (XAG > D3) ; P_{syn},P_{mGluR} (D3 > XAG)

Control reward seeking '15Hz' case: P_{syn},P_{mGluR} & P_{ex} (XAG > molecules > D3).

Importance of path length

The concentration of glutamate at steady state is low in the synapse, and near mGluR (Fig. 1), to prevent excitotoxicity of the NMDA (K_d = 1 μM; Lester and Jahr, 1992) or mGluR receptors (K_d = 183 nM; Schoepp and True, 1992). The extracellular glutamate concentration determined by dialysis experiments is in the range of 5 μM (Lerma et al., 1986; Baker et al., 2002; & Nyitrai et al., 2006). This implies that the glial sheath with its transporters serves to maintain a gradient between the extracellular and synaptic regions.

Immediately after a synaptic release, the transporters on the glia are saturated resulting in most of the synaptic glutamate escaping to the extracellular space. The glutamate gradient then results in an inward flow that continues until the excess glutamate if fully taken up. This exchange is critically dependent on the 'path' followed by the glutamate molecules. Three cases were modeled for configuration 2, with path lengths of 960, 2144, and 3608 nm (by removing (G2, G3, and G4), (G3 and G4), and G4 respectively) and keeping the total number of transporters constant by adjusting density appropriately see appendix for more details. All other parameters were held constant. Table 3.4 lists the estimates of glutamate concentration at the three points, showing significant differences as the path length varies. For instance, the concentration in the synapse and near mGluR varies by 33% and 25% respectively between the path length extremes, highlighting its importance in controlling synaptic concentration and the gradient.

Insights into role of geometry of glial sheaths

The model outputs differ significantly between configurations 1 and 2. The glia in configuration 1 covers 88% of synapse, including the entire postsynaptic side. This configuration is best suited for synapses with a low basal extracellular concentration. Based on NMDA characteristics (Lester and Jahr, 1992) the maximum steady state concentration in synapse can range between 50-150 nM. From the estimates using the proposed computational model, the peak extracellular concentrations achievable by configuration 1 is in the range 0.4 μM-1.5 μM. Configuration 2 is suited for synapses with a high extracellular concentration in the range of 5-10 μM. This was achieved primarily by increasing the path length between the synapse and extracellular space, using the idea of glial folds (Figure 3.2.B), providing appropriate 'isolation' from the extracellular space for the synapse. The number of total transporters used in configuration 2 is low and within physiological bounds.

Other insights derived from the model are as follows: (i) the critical parameters in the system were found to be transporters, diffusion coefficient, path length, molecules and release probability, (ii) after a release most of the molecules escape glial and gradually renter the glia as steady state is achieved, (iii) during high frequency excitation, for the configurations with high transporter density, the number of molecules and release probability has no significant impact on concentration, (iv) CG exchangers maintain the extracellular basal concentration, (v) efficiency of system would increase if CG exchangers and transporters are populated unequally (either cg >> transporters or transporters >> cg), (vi) for configurations with higher basal extracellular concentration

to function we need to isolate the synapse from the extracellular space by increasing the path length, (vii) for high tortuous glial environment the uptake is higher than for the case with less tortuosity, assuming the same transporter concentration, and (viii) less glutamate flux will renter glia if the diffusion coefficients at the transition region are unequal (ideally if diffusion in glia is less than in the outer space).

3.5 CONCLUSIONS

A computational model of feasible glial geometries for a glutamatergic synapse in the PFC-NAc synapse is reported which includes several mechanisms including release of glutamate into the synapse, diffusion of synaptic glutamate into the extracellular space, Glu added by cystine-glutamate exchanger, Glu removal via transporters, and binding to mGluR2/3. Two glial configurations have been proposed and characterized the salient parameters involved in homeostasis. The proposed framework facilitates incorporation of new information, e.g., kinetic constants for specific pathways, as they become available, and thus could serve as an additional tool for investigating glutamate dynamics and homeostasis near synapses. The framework can be used to determine suitable glial geometry for other Glu synapses, in normal or pathological cases, if constraints on transmitter concentrations and physiological ranges for transporters and CG concentrations are available.

3.6 REFERENCES

Anderson KJ, Monaghan DT, Bridges RJ, Tavoularis AL, Cotman CW (1990) Autoradiographic characterization of putative excitatory amino acid transport sites, J Neurosci 38(2):311-22.

Baker DA, Xi ZX, Shen H, Swanson CJ, Kalivas PW (2002) The origin and neuronal function of *in vivo* nonsynaptic glutamate. J Neurosci 22:9134 –9141.

Baker DA, McFarland K, Lake RW, Shen H, Tang XC, Toda S, Kalivas PW (2003) Neuroadaptations in cystine-glutamate exchange underlie cocaine relapse, Nat Neurosci 6:743-9.

Barbour B, Hausser M (1997) Intersynaptic diffusion of neurotransmitter, Trends in Neurosci 20:377-84.

Baude A. (1993) The metabotropic glutamate receptor (mGluR1 alpha) is concentrated at perisynaptic membrane of neuronal subpopulations as detected by immunogold reaction, Neuron 11:771–787.

Bergles DE (1999) Clearance of glutamate inside the synapse and beyond. Current Opinions Neurobiology 9:293–298.

Bowers MS, McFarland K, Lake RW, Peterson YK, Lapish CC, Gregory ML, Lanier SM, Kalivas PW (2004) Activator of G protein signaling 3: a gatekeeper of cocaine sensitization and drug seeking, Neuron 22:269-81.

Capriles N, Rodaros D, Sorge RE, Stewart J (2003) A role for the prefrontal cortex in stress- and cocaine-induced reinstatement of cocaine seeking in rats, Psychopharmacology 168:66-74.

Clements JD, Robin A, Lester J, Tong G, Jahr CE, Westbrook GL (1992) The time course of glutamate in the synaptic cleft, Science 258:1498-1501.

Clements JD (1996) Transmitter time course in synaptic cleft: its role in central synaptic function, Trends in neurosci 19: 163-171.

Colombo JA (2005) Glutamate uptake by rat brain astroglia incubated in human cerebrospinal fluid, Medical Science Monitor 11:BR13-7.

Danbolt NC (2001) Glutamate uptake, Prog in Neurobio. 65:1-105

Diamond JS (2005) Deriving the glutamate clearance time course from transporter currents in CA1 hippocampal astocytes: transmitter uptake gets faster during development, J Neurosci 25(11):2906-16.

Dietrich D, Kral T, Clusmann H, Friedl M, Schramm J (2002) Presynaptic group II metabotropic glutamate receptors reduce stimulated and spontaneous transmitter release in human dentate gyrus, J Neuropharm 42:297-305.

Furuta A, Rothstein JD, Martin LJ (1997) Glutamate transporter protein subtypes are expressed differentially during rat CNS development, J Neurosci 17:8363-75.

Kalivas PW, Volkow N, Seamans J (2005) Unmanageable motivation in addiction: a pathology in prefrontal-accumbens glutamate transmission, Neuron 45:647-50.

Kleinle J, Vogt K, Luscher H -R., Muller R, Senn W, Wyler K and Streit J (1996) Transmitter concentrations profiles in the synaptic cleft: an analytical model of release and diffusion, Biophy. J 71:2413-2426.

Lehre KP, Levy LM, Ottersen OP, Storm-Mathisen J, Danbolt NC (1995) Differential expression of two glial glutamate transporters in the rat brain: quantitative and immunocytochemical observations, J Neurosci 15:1835-53.

Lehre KP, Danbolt NC (1998) The number of glutamate transporter subtype molecules at glutamatergic synapses: chemical and stereological quantification in young adult rat brain, J Neurosci 18:8751-7.

Lehre KP, Rusakov D (2002) Asymmetry of glia near synapse favors presynaptic glutamate escape, Biophy. J 83(1):125-134.

Lerma J, Herranz AS, Herreras O, Abraira V, Martin Del Rio R (1986) In vivo determination of extracellular concentration of amino acids in the rat hippocampus. A method based on brain dialysis and computerized analysis. Brain Res 384:145–155.

Lester, R. A. J., and C. E. Jahr. 1992. NMDA channel behavior depends on agonist affinity. J. Neurosci. 12:635– 643.

Lu L, Hope BT, Shaham Y (2004) The cystine-glutamate transporter in the accumbens: a novel role in cocaine relapse, Trends in Neurosci 27(2):74-76.

McFarland K, Davidge SB, Lapish CC, Kalivas PW (2004) Limbic and motor circuitry underlying footshock-induced reinstatement of cocaine-seeking behavior, J. Neurosci 24:1551-60.

Nicholson C and Phillips JM (1981) Ion diffusion modified by tortuosity and volume fraction in the extracellular microenvironment of the rat cerebellum, J Physio. 321: 225-257

Nyitrai G, Ke´kesi KA, Juha´sz G (2006) Extracellular level of GABA and Glu: *in vivo* microdialysis-HPLC measurements. Curr Top Med Chem 6:935–940.

Pendyam S, Mohan A, Knackstedt LA, Melendez R, Kalivas PW, Nair SS, Computational model of extracellular glutamate in the nucleus accumbens predicts neuroadaptations by chronic cocaine, Journal of Neuroscience (in review).

Peters YM, O'Donnell P, Carelli RM (2005) Prefrontal cortical cell firing during maintenance, extinction, and reinstatement of goal-directed behavior for natural reward, Synapse 56(2):74-83.

Rusakov DA, Kullmann DM (1998a) Extrasynaptic glutamate diffusion in the hippocampus: ultrastructural constraints, uptake, and receptor activation, J Neurosci 18:3158-70.

Rusakov DA and Kullman DM (1998b) Geometric and viscous components of the tortuosity of the extracellular space in the brain, Proc. Nat. Acad. of Sci. 95:8975 - 8980.

Rusakov DA (2001) The role of perisynaptic glial sheaths in glutamate spillover and extracellular Ca^{2+} depletion, Biophys J. (81):1947-1959.

Schoepp DD, True RA (1992) 1S-3R-ACPD-sensitive (metabotropic) [^{3}H] glutamate receptor binding in membranes. Neurosci letts 145:100-104.

Schoepp DD, Jane DE, Monn JA (1999) Pharmacological agents acting at subtypes of metabotropic glutamate receptors. Neuropharmacology 38:1431–1476.

Seamans JK, Yang CR (2004) The principal features and mechanisms of dopamine modulation in the prefrontal cortex, Progress in Neurobiology 74:1-58.

Sun W, Rebec GV (2005) The role of prefrontal cortex D1-like and D2-like receptors in cocaine-seeking behavior in rats, Psychopharmacology 177:315-23.

Sykova E (2004) Extrasynaptic volume transmission and diffusion parameters of the extracellular space, J Neurosci 129:861-876.

Takahashi M, Sarantis M, Attwell D (1996) Postsynaptic glutamate uptake in rat cerebellar Purkinje cells, Journal of Physio 497:523–530.

Thorne RG, Nicholson C (2006) In vivo diffusion analysis with quantum dots and dextrans predicts the width of brain extracellular space, Proc. Natl. Acad. of Sci. 103:5567-5572.

Trommershauser J, Schneggenburger R, Zippelius A, Neher E (2003) Heterogeneous Presynaptic release probabilities: functional relevance for short-term plasticity, Biophy. J 84:1563-69.

Uteshev VV and Pennefather PS (1996) A mathematical description of miniature postsynaptic current generation at central nervous system synapses, Biophysical Journal 71: 1256 -66.

Wang Y, Rudnick PA, Evans EL, Li J, Zhuang Z, Devoe DL, Lee CS, Balgley BM. (2005) Proteome analysis of microdissected tumor tissue using a capillary isoelectric focusing-based multidimensional separation platform coupled with ESI-tandem MS, Annals of Chem 77(20):6549-56.

Warr O, Takahashi M, Attwell D (1999) Modulation of extracellular glutamate concentration in rat brain slices by cystine-glutamate exchange, J Physio. 514:789-93.

Wheatley DN (1998) Diffusion theory, the cell and the synapse, BioSystems 45:151-163.

Wyatt I, Gyte A, Simpson MG, Widdowson PS, Lock EA (1996) The role of glutathione in L-2-chloropropionic acid induced cerebellar granule cell necrosis in the rat, Arch. of Tox. 70(11):724-35.

3.7.TABLES

Table 3.1.a Ranges for parameter values used in model, and constraints.

Parameter	**Range of Values (citation)**	**Model Value** [a]
Diffusion coefficient[b] (**(**$\mu m^2/ms$)	0.05 – 0.75 (Rusakov and Kullmann, 1998)	see 'b' below
k_1 ($M^{-1}ms^{-1}$)	10^4 (Lehre and Rusakov, 2002)	10^4
k_{-1} (ms^{-1})	0.2 (GLAST/GLT; Lehre and Rusakov, 2002)	0.2
k_2 (ms^{-1})	0.1 (Lehre and Rusakov, 2002)	0.1
No. of molecules per release	4,700 - 80,000 (Bruns and Jahn, 1995)	10000
Intersynaptic distance (μm)	2-20 (Rusakov, 2001)	2
K_d (μM)	0.1-0.3 (Schoepp and True, 1992)	0.187
Maximum release probability	0.1-0.5 (Trommerhauser et al., 2003; Billups et al., 2005; Volynski et al., 2006)	0.4 (max)
Transporter conc. (molecules/μm^2)[c]	550-3780 (Bergles and Jahr, 1997; Lehre and Danbolt, 1998; Colombo 2005)	see 'c' below
CG (moles/min)[d]	8 - 25 x 10^{-18} (Warr et al., 1999)	1.1 x 10^{-17}

[a] Values used to populate model 3 in Figure 3.1 [b] D_1= 0.125, D_2=D1/0.12 , D_3= 0.06, D_4=D_3

[c] surface density (molecules/μm^2) of transporters was distributed as follows: G1a-1094, G1b-1090, G2a-1087, G2b-971, G3a-604, G3b-465, G4a-0, G4b-0

[d] CG was distributed uniformly in eight compartments of G4b: (i=12, j = 2-8)

3.1b. Model constraints

Parameter	**Control**	**Reference**
Glutamate in Pex (μM; basal)	5.6 ± 1.0	Baker et al., 2003; Szumlinski et al., 2006
Peak glutamate in Pex (μM; during reward seeking)	5.6 ± 1.0	McFarland et al., 2003, 2004.
Glutamate in P_{syn} Transporter density (μm^3)	50-150 nM 550-3780	Clements, 1996 Colombo,2005; Danbolt,2001
CG (moles/min)	1.1 x10^{-17}	Baker et al., 2003
Maximum release probability	0.24 (basal) 0.20 (reward)	Xi et al., 2002
Firing freq (Hz) (basal)	2	Sun and Rebec, 2006; Trantham et al., 2002

Table 3.2. Optimal parameter values and corresponding estimates for both configurations.

	Configuration1	**Configuration2**
Molecules/release	10000	10000
Transporter density (molecules/$\mu m^{2)}$	1804-4620	465-1094
CG production (moles/min)	4.3 x 10^{-17}	1.1 x 10^{-17}
Diffusion (D3) in the glial region (μm^2/ms)	0.01*	0.06
P_{ex} (μM)	5.12	5.08
P_{mGluR} (μM)	0.708	0.184
P_{syn} (μM)	0.311	0.118

* note: D3 is significantly smaller than its lower bound even to achieve this partial match with requirements.

Table 3.3. Concentrations at P_{ex}, P_{mGluR} and P_{syn} observed with variation in primary parameters.

		Configuration 1			Configuration 2		
		P_{syn}	P_{mGluR}	P_{ex}	P_{syn}	P_{mGluR}	P_{ex}
Diffusion Coefficient in Glia	(+) 10%	9.80%	2.24%	−2.19%	13.10%	9.80%	−4.40%
	(−) 10%	9.90%	2.50%	−2.38%	15%	12%	−4.90%
Total Transporters (XAG)	(+) 10%	−10.20%	−9.13%	−7.90%	−4.80%	−18.7%	−21.2%
	(−) 10%	−8.41%	−10.8%	−9.69%	−5.23%	−19.0%	−20.9%
Molecules per release	(+) 10%	–	–	–	14.3%	13.9%	14.8 %
	(−) 10%	–	–	–	15.5%	14.02%	15.6%
Release Probability	(+) 10%	–	–	–	1.2%	3.2%	6.73%
	(−) 10%	–	–	–	1.5%	3.13%	5.23%

Table 3.4. Variation of gradient with path length, with constant transporter molecules.

Path Length (nm)	P_{syn} (μM)	P_{mGluR} (μM)	P_{ex} (μM)	Gradient(μM)
a) 960	7.31E-07	1.31E-06	3.18E-06	2.45E-06
b) 2144	3.60E-07	5.06E-07	4.43E-06	4.07E-06
c) 3608	2.43E-07	3.21E-07	5.00E-06	4.76E-06

3.8. FIGURES

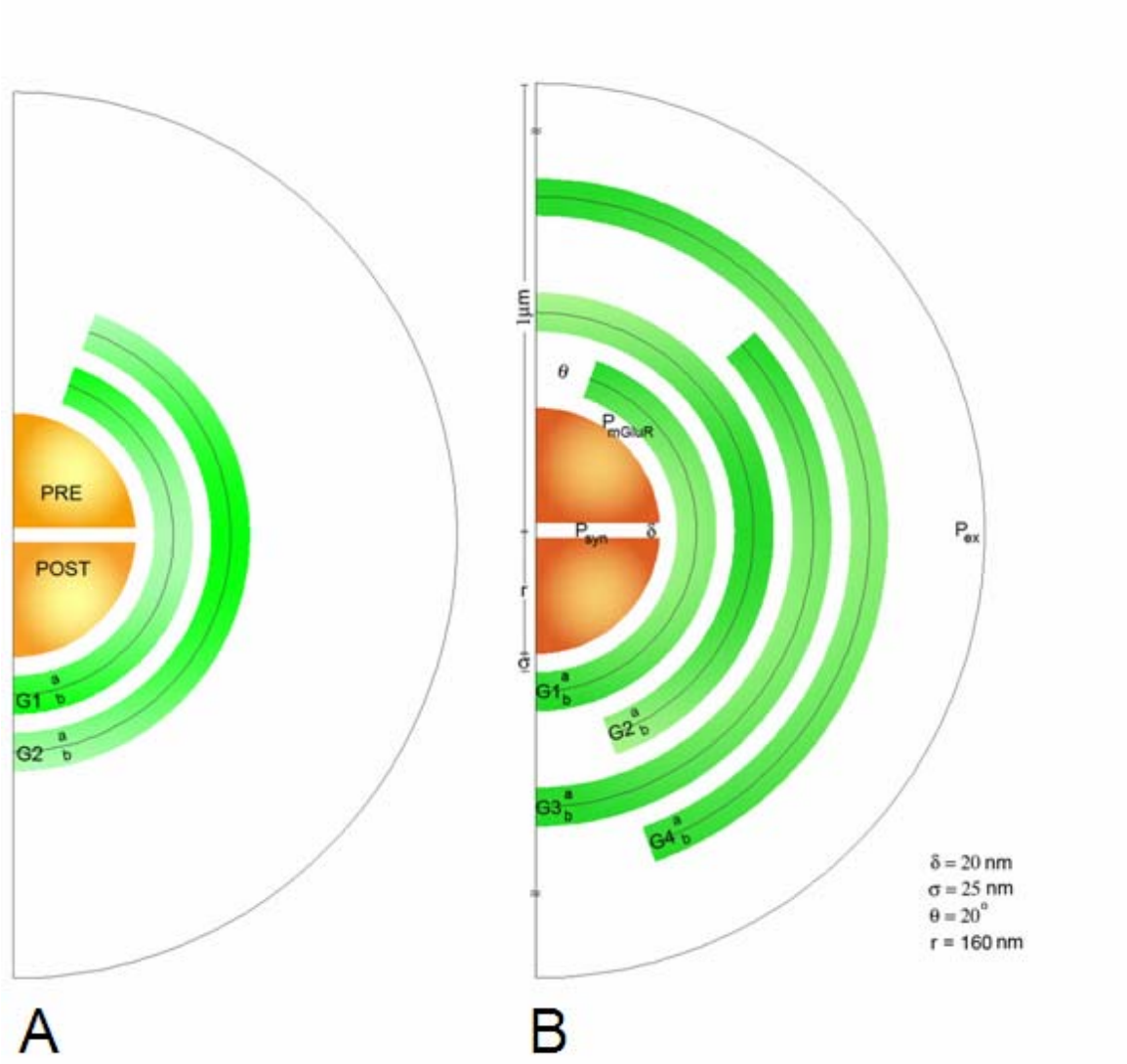

Figure 3.1. Proposed glial configurations to study glutamate homeostasis in the perisynaptic space around the PFC-NAc synapse. Model includes glutamate transporters (XAG) and cystine glutamate exchangers (xc-) in glial regions (green) in varying concentrations to study transients and steady state characteristics.

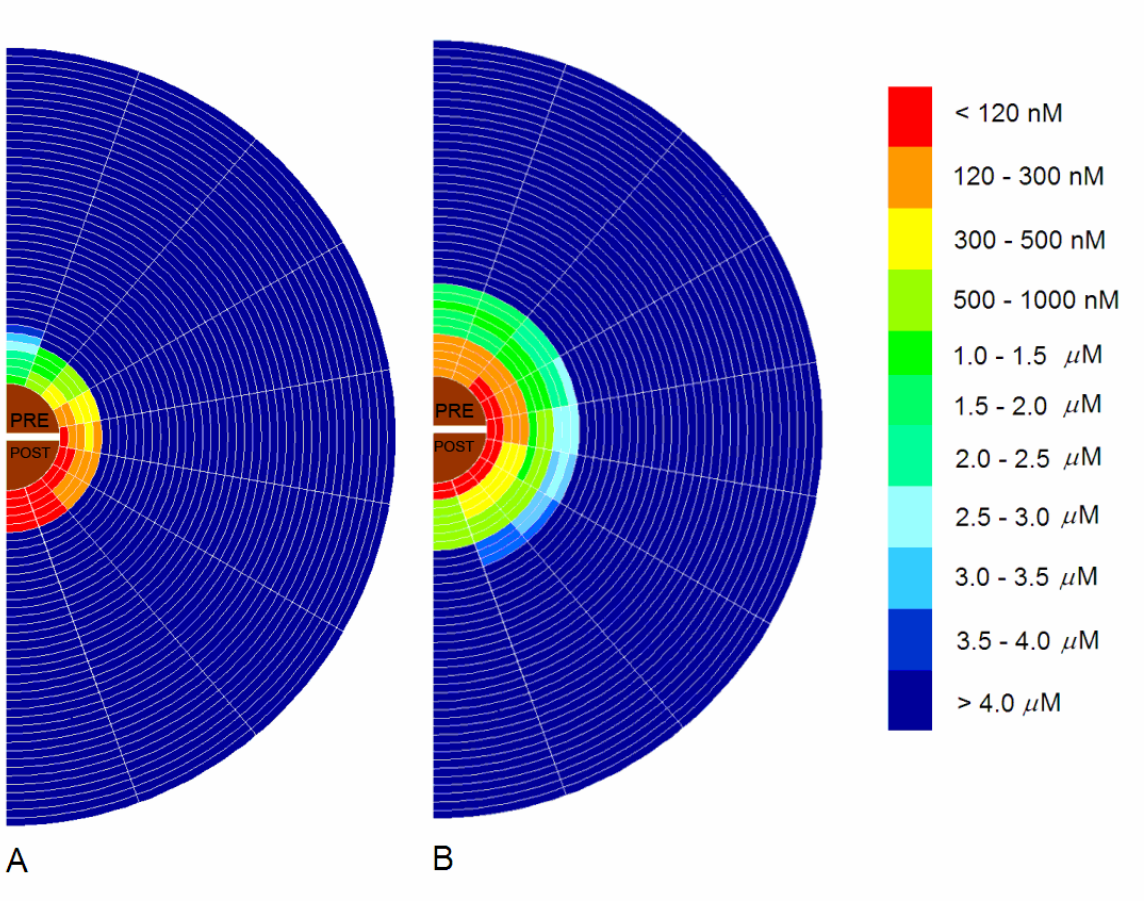

Figure 3.2. Steady state concentrations observed in all compartments for configurations 1 (A) and 2 (B).

Note: The diffusion coefficient 0.015 $\mu m^2/ms$ (< lower bound of D) was needed in configuration 1 to attain a concentration of 50-150 nM at P_{syn}.

CHAPTER 4
MODELING THE EXTINCTION OF FEAR IN AMYGDALAR CIRCUITS

4.1 ABSTRACT

An artificial neural network model is developed of the various brain regions involved in fear extinction. This includes the amygdala, hippocampus and ventro-medial prefrontal cortex. Hebbian synaptic plasticity is implemented into the excitatory and inhibitory receptor mediated synapses to model learning, using electrophysiology and imaging data from rats. The model is used to develop insights into the mechanisms of extinction and the important role of vmPFC in the recall of extinction after a long delay.

4.2 INTRODUCTION

The brain region described as amygdala, the main component of the fear circuit, consists of several nuclei with distinct functional traits. These nuclei groups include the basolateral complex, the centromedial nucleus and the cortical nucleus. The basolateral complex can be further subdivided into the lateral, the basal and the accessory basal nuclei. The description of the system below is adapted from Hummos (2008).

The amygdala receives input from divergent areas spanning all sensory levels (McDonald 1998). Sensory information from all modalities except for olfactory, converge into the different thalamic nuclei and is then relayed to different brain areas.

The amygdala receives input from the thalamic nuclei through the thalamo-amygdalar connections. The thalamic input reaches the amygdala relatively early in the hierarchy of sensory information processing, allowing it to quickly supply the amygdala with low-level sensory information. The thalamo-amygdalar connections where shown to exhibit NMDA-dependent long-term potentiation (LTP).

Inputs to the amygdala.

Visual information from the retina reach the Lateral Posterior thalmic nucleus (LP), and the dorsal lateral geniculate nucleus (LGD) (Shi and Davis, 2001). Destruction of LP and LGD impaired visual fear conditioning (Shi and Davis 2001). The LP was shown to project directly to the lateral amygdaloid nucleus, while LGD projects to the primary visual cortex V1 and then indirectly to the amygdala through cortical cascades. The high-order visual association temporal cortical area TE2 sends robust projections to the amygdala (Mascagni et al., 1993; Shi and Cassell, 1997).

Auditory information, on the other hand, reaches the medial aspect of the medial geniculate nucleus (MGm), ventral aspect of medial geniculate nucleus (MGv) and the posterior intralaminar nucleus (PIN). All areas project to the auditory cortical areas. MGm and PIN also project directly to the amygdala, and were shown to be zones of convergence of auditory inputs (CS) and somatosensory information (US). The amygdala also receives a higher level of information as input from all sensory cortical areas (Gray et al.,1981). In all mammals studied the most robust cortico-amygdalar projections originated from the higher-order association sensory cortices, which in turn receives information through a cascade of cortico-cortical projections that originate in the primary cortices (Turner et al. 1980). Lesion studies of the cortico-

amygdalar tracts suggested that the primary function of these projections is to endow sensory representations in the cortex with emotional and motivational significance.

In addition to modality-specific inputs from the thalamus and unimodal cortical areas, the amygdala also receives highly-processed multimodal afferents from the prefrontal cortex, perirhinal cortex and hippocampus.

Output of the amygdala.

The Central nucleus of the amygdala (CE) is the fear response center that orchestrates the fear reaction and is the main output area of the amygdala. Specifically, the medial part of the CE (CEm) sends numerous projections to downstream areas involved in the manifestation of the fear response. It sends projections to periacquiductal gray, locus cerelulus, raphe, hypothalamus, etc. The basolateral amygdala, or more specifically the lateral amygdala, was shown to receive input from divergent areas of the brain, and more interestingly, a consistent body of evidence established that single neurons within the LA receive information of conditioned and unconditioned stimuli (Sah et al. 2003; Rodrigues et al. 2004). Converging evidence has shown the LA to be a critical site for the acquisition and retention of conditioning training. Lesion studies revealed that inactivation of LA impairs fear conditioning (LeDoux, 2000). Pharamacological inactivation and electrophysiological recording studies also arrived at a similar conclusion.

The fear circuit model held the LA as the processor that receives inputs from sensory areas to process it and then to relay it to the central nucleus, which functions to activate several downstream brain centers responsible for the various manifestations of the fear reaction (LeDoux, 2000; Davis and Whalen, 2001; Maren 2001). Following

mounting evidence, the central nucleus was shown to receive projections from most of the areas that the LA receives projections from. The emerging view considers the central nucleus as a more active component in processing and learning conditioned fear associations (Paré *et al.,* 2004; Samson & Paré, 2005), with the LA acting to disinhibit the CE. Both CE and LA receive connections from the auditory cortex (McDonald 1998) and display long-term potentiation following high-frequency stimulation of thalamic inputs (Samson and Pare, 2005). The CE also receives pain information from the spino (trigemino)-parabrachio-amygdaloid pathway (Bernard and Besson, 1990; Jasmin et al., 1997). According to Wilensky *et al.* (2006), the inactivation of the central nucleus had more impact on conditioning learning than the inactivation of the LA.

Role of intercalated cell mass (ICM).

As indicated above, LA was thought to directly send glutamatergic connections to the CEm thereby activating its brainstem-projecting neurons. Arguing against such possibility was the finding that LA has little, if any, direct communication with CEm neurons. Pare et al.(2004) suggested a more complex picture. The intercalated cell mass is a group of GABAergic inhibitory neurons interposed between the basolateral amygdala and the medial amygdala. The ICM neurons are arranged in an interesting pattern. The more lateral neurons send inhibitory projections to the more medially located ones. The medial aspect of ICM sends inhibitory connections to the CEm. The LA sends glutamatergic stimulation exciting the lateral aspects of ICM, increasing its inhibition of the medial aspect of ICM. The end result is a decrease in the inhibition of the medial ICM on the CEm neurons allowing them to be more responsive to stimuli. This added layer of complexity most probably allows the CEm to be tightly controlled and constantly under

check. It also provides a suitable mechanism for other areas to modulate the transmission of signals between the LA and the CEm.

Extinction.

Pavlov (1927) also studied the phenomenon of extinction, where the CS no longer induces a CR following repeated presentation of CS in the absence of US. Initially it was believed that extinction training leads to weakening of the memory associating the CS and US. Pavlov suggested a different hypothesis. He noticed that the simple passage of time was adequate for the "spontaneous recovery" of the original CR in response to the CS. In addition he also noted that exposure to US alone or other stressful stimuli leads to the "reinstatement" of the CS-US association expression. These observations strongly suggested that the initial CS-US memory is still intact, and that extinction training leads to the formation of an inhibitory CS/No-US memory. Stronger convincing evidence was found in the fact that once the animal is removed from the context in which extinction training took place, renewal of the CR to CS was observed. Despite the early recognition that some area in the brain harbored the extinction memory, no strong candidate areas were identified for many years. Morgan et al. (1993) showed that rats with vmPFC lesions were able to acquire fear conditioning normally, and were able to extinguish normally early after the extinction training, however, they showed deficits in recalling extinction 24 hours later. This suggested that vmPFC plays a crucial role in the consolidation of across sessions extinction recall. Following initial lesion studies reports, convincing evidence came from electrophysiological recordings of neuronal activity. Recordings from single neurons of the Infra-Limbic (IL) part of the rat vmPFC showed

that these neurons responded to CS presentation 24 hours after initial extinction training, but not during acquisition or extinction training. Moreover, electrical stimulation of the vmPFC in rats decreased the expression of fear response.

Revisiting the intra-amygdalar circuits, it was noted that the vmPFC sends projections that heavily innervate the ICM of the amygdala. This organization places the vmPFC in a suitable position to signal extinction memory through its excitatory projections to the ICM neurons, and by modulating the activity of the inhibitory ICM neurons, the transmission of information from LA to CEm can be tightly controlled (Quirk et al. 2003). Additionally, studies revealed that extinction training decreases the CS-evoked potential in many LA neurons (Quirk et al. 1995; Repa et al. 2001). Direct inhibitory signals from vmPFC or excitatory signals to the inhibitory inter-neurons of the LA are proposed mechanisms.

More recent evidence pointed to a more complex interplay between the amygdala and the hippocampus along with the vmPFC as an extended circuit that regulates maintaining and expressing the extinction memory. The current hypothesis is that these three areas work in concert to suppress the expression of fear memory to extinguished stimuli in the right context (Milad et al., 2007). Several interesting phenomena shed light on contextual-modulation of fear response. Context-shift effect describes the decrease of the CR when the animal encounters the CS in a context other than the context of the original conditioning training (Gordon et al., 1981). The other phenomena is renewal, the expression of a CR to a CS in a context other than the context of initial extinction training (Bouton and King, 1983; Rauhut et al., 2001). An interesting observation was that the CR renewed by changing context is not as strong as the CR exhibited by subjects that have

never received extinction training (Bouton and King, 1983), a fact that strongly suggests that extinction is only partly context-specific (Bouton et al. 2006). Electrolytic lesions of the dorsal hippocampus prior or after extinction training impaired the renewal of conditioned response when the context was changed (Ji and Maren 2005).

Several behavioral studies of renewal facilitated understanding the nature of context modulation. The initial thoughts were that context is just a second CS that acquires excitatory or inhibitory associations with fear response. Current evidence presents a more complex picture where direct association between context and US is neither sufficient nor necessary to modulate fear response. The context appears to influence the meaning of the CS, whereas the CS-US association is activated in one context and the CS-no US is activated in another (Bouton, 1993).

Contextual modulation of extinction memory.

The last input to the network is the context information. In the brain of the rat, context is derived from multi-modal inputs converging into the hippocampal apparatus where binding of these elements leads to a unitary representation of the surrounding environment. Context derivation probably also involves navigational sense, and extensive cortical process to infer location from sensory inputs.

4.3. HYPOTHESIS

Simulations of Fear Extinction using Integrate-and-Fire Neuronal Models

Classical fear conditioning is an experimental model used to study how organisms learn to predict danger from previous experiences. In this model, repeating presentations of a conditioned stimulus (US), such as a tone, paired with an aversive unconditioned stimulus (US), such as electric shock, elicits autonomic and behavioral fear responses such as freezing in the subsequent presentations of tone only. Once acquired, conditioned fear associations are not always expressed. Repeated presentation of the tone CS in the absence of US causes conditioned fear responses to rapidly diminish, a phenomenon termed fear extinction.

The neural mechanisms of fear extinction are not well understood, and a neural analysis of extinction and inhibition is still in its infancy (for a good review, see Myers and Davis, 2002). To better understand the neural mechanisms of fear extinction, we are developing neuronal network models with relevant brain structures, including lateral amygdala (LA), basolateral amygdala (BL), central amygdala (CE), intercalated cell mass (ITC), vmPFC, and hippocampus (Fig 4.1). Each structure has a population of neurons which are modeled as integrate-and-fire models, which is much more neurologically realistic than artificial neural network model by generating spike behaviors. Spike timing dependent plasticity (STDP) is implemented in the excitatory connection between thalamus-to-LA, BL-to-ITC, and mPFC-to-ITC.

The LA receives convergent tone and shock inputs from the thalamus. The simulation includes sensitization (10 tones unpaired with 10 shocks), conditioning (10 tones paired with 10 shocks) and extinction phases (30 pure tones). We are interested in

how the auditory information is processed by this circuit, including (1) the role of ITC neurons in fear extinction; (2) how vmPFC regulates fear after it is learned and (3) how fear and extinction can be learned with the STDP rule. Lesion experiments will be simulated by damage of the vmPFC and the BL.

Two context-dependent phenomena in fear conditioning have received considerable recent interest. One is context specificity or the context-shift effect, the decrease of conditioned responding (CR) when the CS is tested in a context different from the one where it had been paired with the US. The other effect is renewal, the recovery of CR in the training context after extinction in another context. Context specificity and renewal are generally believed to involve hippocampus function. The model will also test different existing hypotheses regarding context specificity and renewal.

4.4 METHODS

The cortex has connections to all major areas of the model and will hold representation of all the information acquired from the environment or processed by different areas. The output layer of the cortex will be divided into several parts. The visual part of the cortex will store visual information from the thalamus, the somatosensory cortex will store US information, and the vmPFC will store a representation of the LA activity. The frontal cortex will carry a representation of context (multi-modal information) which is given to the model as an input. Following re-entrant activity with the input layer of the cortex layer and the hippocampus, past memories will attract the current pattern to a stable state representing an old memory and will complete any missing parts of the memory.

The vmPFC in our model will take inputs from the LA as an activating signal to focus attention and will have its major input from the cortex giving it access to the current representation of the world. In addition, it will form a re entrant activation with the hippocampal neurons so that the state of the vmPFC when exposed to the same outside environment will be retrieved from memory and will influence the activity of vmPFC attracting it towards that remembered state. What is also expected of this design is to employ one of the strongest features of neural networks, generalization. Since the representation of the world is presented as input and since parts of the world tend to recur at different combinations, hopefully the network will be able to build generalizations from old experiences and improve its ability to categorize new experiences more correctly and promptly.

This design will allow the model to account for contextual-modulation and other related features. It will allow the meaning of a CS to change in different context because simply the CS in context A has a different representation than CS in context B and to the network, these are different input patterns. Nevertheless, the generalization between the similar portions of the two inputs (the CS) can still have its effect on processing if high enough. The design will also reproduce contextual-shifts where a CS exhibits a stronger CR when presented in its original context. So if the amygdala thinks the current environment might be biologically important it helps activate the vmPFC to make its own assessment. The vmPFC runs its assessment dependent on highly processed cortical information and accesses the hippocampus for past experiences and encounters with the objects in the current environment.

Modeling

The computational model will be developed using PDP++ (an open ended software from developed initially at Carnegie Mellon University, and now at the University of Colorado at Boulder). PDP++ is designed to create complex, sophisticated models of the brain and cognitive processes. The proposed model will be developed in four steps: i) create the network, ii) create the environment, iii) train and test the network, and, iv) analyze the results and iterate as appropriate.

The network shown in Figure 4.2 will be created and adding layers such as thalamus, cortex, hippocampus and amygdala to the network container. The layer is a collection of basic computational elements, or units, of networks. After the creation of layers, projection classes are created to interconnect the layers.

When the network is created an environment object is created that contains all the information that specifies the kinds of stimuli or patterns that the network will be tested or trained on. Then we actually train and test the network using Processes objects that orchestrate and coordinate the interactions between different object types in order to carry out particular tasks. Processes objects will contain the training and testing steps. The output from PDP++ will be seen in objects called Logs. Logs provide a convenient method of recording information from the processes.

This represents the research done so far as part of the MS program, and will be continued in the Ph.D. program.

4.5 REFERENCES

Bouton ME, King DA (1983) Contextual control of the extinction of conditioned fear: tests for the associative value of the context. J Exp Psychol Anim Behav Process 9:248-265.

Bouton ME, Westbrook RF, Corcoran KA, Maren S (2006) Contextual and temporal modulation of extinction: behavioral and biological mechanisms. Biol Psychiatry 60(4):352-60.

Davis M, Whalen PJ (2001) The amygdala: vigilance and emotion. Mol Psychiatry 6, 13–34.

Gray, JA (1981) Anxiety as a paradigm case of emotion. Br. Med. Bull. 37:193–197.

Hummos, A (2008) Neural correlates of fear circuit, Internal report, Dept. of Psychiatry, University of Missouri-Columbia.

Jasmin L, Burkey AR, Card JP, Basbaum AI (1997) Transneuronal labeling of a nociceptive pathway, the spino-(trigemino-) parabrachio-amygdaloid, in the rat. J Neurosci 17:3751–3765.

Ji J, Maren S (2005) Electrolytic lesions of the dorsal hippocampus dirsupt renewal of conditional fear after extinction. Learn Mem 12:270-276.

LeDoux JE (2000) Emotion circuits in the brain. Annu Rev Neurosci. 23:155-184.

Maren S (2001). Neurobiology of Pavlovian fear conditioning. Annu Rev Neurosci 24, 897–931.

Mascagni F, McDonald AJ, Coleman JR (1993) Corticoamygdaloid and corticocortical projections of the rat temporal cortex: a Phaseolus vulgaris leucoagglutinin study. J Neuroscience 57(3):697-715.

McDonald AJ (1998) Cortical pathways to the mammalian amygdala. Prog Neurobiol 55:257–332

Milad MR, Wright CI, Orr SP, Pitman RK, Quirk GJ, Rauch SL (2007) Recall of fear extinction in humans activates the ventromedial prefrontal cortex and hippocampus in concert. Biol Psychiatry 62(5):446-54.

Morgan MA, Romanski LM, Ledoux JE (1993) Extinction of emotional learning: contribution of medial prefrontal cortex, Neurosci Lett 163, pp. 109–113.

Pare D, Quirk GJ, Ledoux JE (2004) New vistas on amygdala networks in conditioned fear. J Neurophysiol 92:1-9.

Pavlov I (1927) Conditioned reflexes. London: Oxford UP.

Quirk G, Repa C, LeDoux JE (1995) Fear conditioning enhances short-latency auditory responses of lateral amygdala neurons: parallel recordings in the freely behaving rat. Neuron 15: 1029-1039.

Quirk GJ, Likhtik E, Pelletier JG, Pare D (2003) Stimulation of medial prefrontal cortex decreases the responsiveness of central amygdale output neurons. J Neurosci 23:8800-8807.

Repa JC, Muller J, Apergis J, Desrochers TM, Zhou Y, LeDoux JE (2001) Two different lateral amygdala cell populations contribute to the initiation and storage of memory. Nat Neurosci. 4(7):724-31.

Rodrigues S, Schafe G, LeDoux J (2004) Molecular mechanisms underlying emotional learning and memory in the lateral amygdala. Neuron 44:75-91.

Sah P, De Armentia ML (2003) Excitatory synaptic transmission in the lateral and central amygdala. Annals of the New York Academy of Sciences 985 (1), 67–77.

Samson RD, Paré D (2005) Activity-dependent synaptic plasticity in the central nucleus of the amygdala. J Neurosci 25:1847–1855.

Shi CJ, Cassell MD (1999) Perirhinal cortex projections to the amygdaloid complex and hippocampal formation in the rat. J Comp Neurol 406: 299–328.

Shi C, Davis M (2001) Visual pathways involved in fear conditioning measured with fear-potentiated startle: Behavioral and anatomic studies. J Neurosci 21(24):9844–9855.

Turner BH, Mishkin M, Knapp M (1980) Organization of the amygdalopetal projections from modality-specific cortical association areas in the monkey. J. Comp. Neurol. 191, 515-543

Washburn MS, Moises HC (1992) Electrophysiological and morphological properties of rat basolateral amygdaloid neurons *in vitro*. J Neurosci 12:4066-4079.

Wilensky AE, Schafe GE, Kristensen MP, LeDoux JE (2006) Rethinking the fear circuit: the central nucleus of the amygdala is required for the acquisition, consolidation, and expression of pavlovian fear conditioning. J Neurosci 26:12387–12396.

4.6 FIGURES

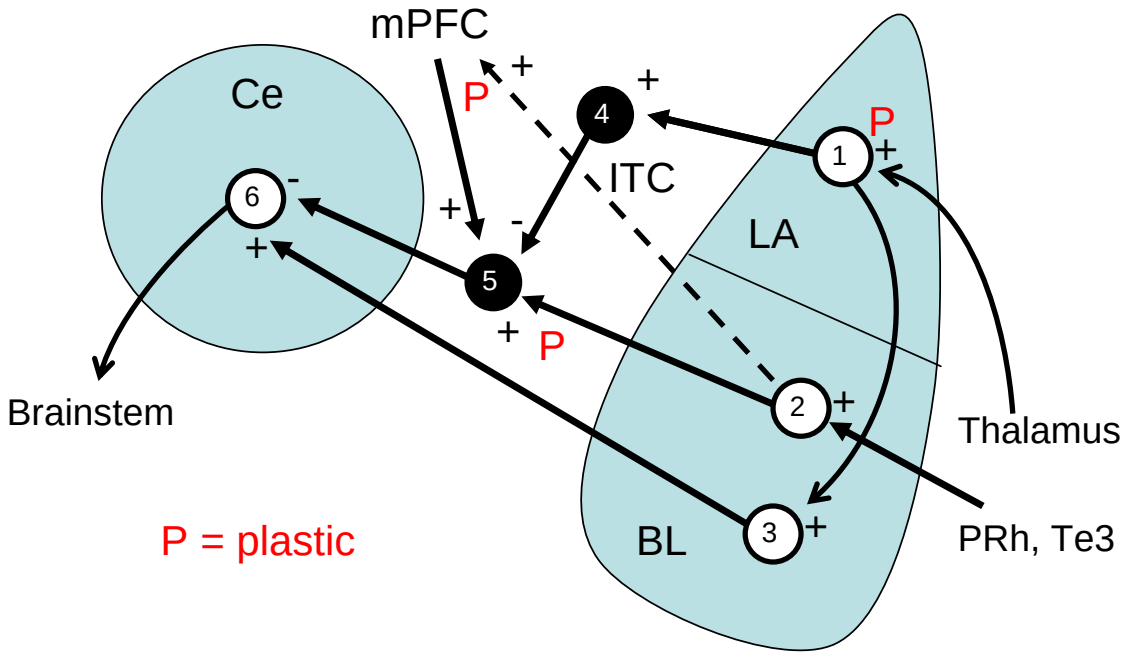

Figure 4.1. Fear extinction circuit

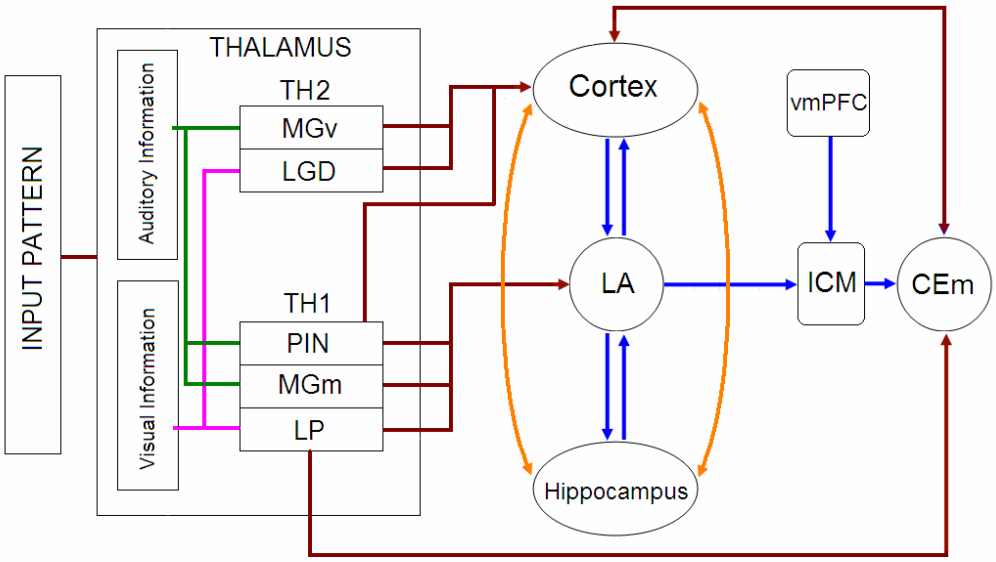

Figure 4.2. The visual and auditory information reaches lateral amygdaloid nucleus either through cortical cascades or by direct projection. The amygdala sends the output through ICM (group of GABAergic inhibitory neurons) to the output area CE (Central nucleus of the Amygdala). The amygdala, the hippocampus and the vmPFC control extinction.

CHAPTER 5

Summary and future research

5.1 SUMMARY

Computational models at a molecular level were developed to model glutamate homeostasis in extracellular region of nucleus accumbens with the larger goal of studying the effects of chronic cocaine abuse. At the network level, a framework to study the role of vmPFC in the extinction in fear circuits is proposed, using artificial networks and PDP++ software.

The key points in each chapter are summarized below.

Chapter 2

- A biologically relevant model of a PFC-Nac synapse that incorporates both synaptic and nonsynaptic glutamate release and homeostatic regulation of synaptic release via stimulation of mGluR2/3 autoreceptors was developed.
- Model accurately predicted the basal levels of extracellular glutamate measured by microdialysis, as well as the levels of glutamate in the vicinity of mGluR2/3 that provides inhibitory tone on synaptic released.
- The model was used to study plasticity induced in the accumbens due to cocaine pathology. It successfully predicted the dysregulation of extracellular glutamate accompanying cocaine-seeking, by accurately forecasting a down-regulation of XAG.

Chapter 3

- ❖ The computational framework for homeostasis was used to determine feasible geometries for the glial sheaths surrounding the synapse.
- ❖ The effect of glial geometry on glutamate homeostasis was characterized, including its ability to sustain gradients in concentration.
- ❖ Parametric and robustness studies were conducted to rank the importance of the various parameters in the system.

Chapter 4

- ❖ Building on the cellular level modeling of fear circuit performed by our group, a network level model is proposed for the circuit including the amygdala (basal, lateral, and central nuclei), hippocampus, and vmPFC to study their relative roles in the extinction of fear.

5.2 FUTURE RESEARCH

Chapter 2

1) The computational model was implemented as a continuum model in the paper, the model would be developed as a Monte Carlo similuation using MCELL software.
2) The glutamatergic synapse can be used with additional neurotransmitters such as dopamine to study their interactions.
3) By populating many synapses together we can study the phenomena of crosstalk, where a synapse affects neighboring ones.
4) Characterize tortuosity for models that have impermeable glial sheaths.

Chapter 3

1) Based on the parametric studies a reduced order model can be developed that emulates the complex nonlinear model with reduced number of parameters.
2) Characterize glutamate uptake and formulize a constant that predicts the gradient. This constant will help in creating models based on the extracellular space.
3) Further analyze the glial configurations to develop a glial architecture that is more physiological in appearance and shape.

Chapter 4

1) The role of vmPFC in extinction of fear needs to be analyzed using the proposed network model using artificial neural nets and PDP software.

APPENDIX A

CHARACTERIZE PATH LENGTH BASED ON UPTAKE AND TRANSPORTER DISTRIBUTION.

It has been observed that, with same number of total transporters and different distribution leads to varied spectrum of concentrations. In order to characterize this property, three configurations with different transporter distributions were considered as shown in Figure 1. These configurations have same parametric set except for distribution and number of sheaths.

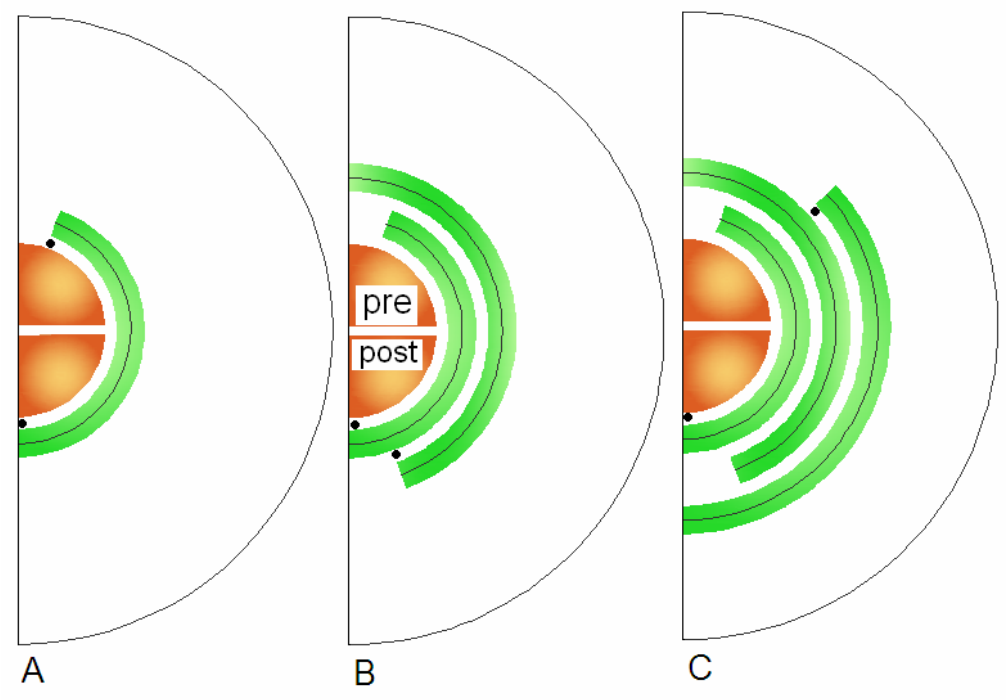

Figure 1. To verify the effect of path length in perisynaptic space , three configurations as shown here were considered. Note that the path length for A,B and C are 960 nm, 2144 nm, and , 3608 nm respectively. Path length is measured from the base of post-synapse (distance between black dots in each case).

The density of XAG is non-uniform, and glial membranes that face neuropil have a higher expression of transporter than membrane surfaces facing other glia (Cholet et al., 2002). The transporters density located in glial leaflets surrounding dendritic spines and dendrite and/or axonal elements of asymmetrical (glutamatergic) axo-dendritic synapses was around 73% of total concentration. XAG are expressed with a high density in the hippocampus, with surface density ranging from 2500-10,800 molecules/μm^2 (Bergles and Jahr, 1997; Lehre and Danbolt, 1998). Based upon glutamate uptake assays (Colombo, 2005) and transporter binding density (Danbolt, 2001) it was estimated that surface density values for the nucleus accumbens is 22-35% (550-3780 molecules/μm^2) of the value in the hippocampus and cortex.

Assumptions of study:

- The number of molecules per release and release probability are same in each case (10000 molecules@ 0.24 R.P.) .
- The total cg production was fixed at 1.1 x 10^{-17} moles/min in all three cases.
- The total transporters in the system same but there distribution varied as follows
    - Configuration A transporter densities are G1a, and G1b are 8000 and 4500 molecules/ μm^2 respectively.
    - Configuration B transporter densities are G1a, G1b, G2a, and G2b are 4000, 2500, 2000 and 1400 molecules/ μm^2 respectively.
    - Configuration C transporter densities are G1a, G1b, G2a, G2b, G3a, and G3b are 3300, 2000, 1650, 1000, 600 and 400 molecules/ μm^2 respectively.

Transporters numbers used for the three configurations are based on following studies

- Configuration A (with glial sheaths G1a and G1b see figure 1a)
    - Total transporter molecules populated on G1a should be at least three times greater than G2b, to maintain a synaptic concentration that is 25.6 % of extracellular concentration.
    - Total transporters in G1a can exceed thrice G2b, if this number can be arranged in G1a without exceeding the transporter density of 550-3780 molecules/μm^2 (Colombo, 2005).
    - Surface area of the sheaths G1a and G2b are in the ratio 9:16.
    - Other combinations of transporter distributions in G1a and G1b are

Ratio	P_{syn} (μM)	P_{mGluR} (μM)	P_{ex} (μM)	(P_{ex}/P_{syn}) *100
1:1	1.94E-06	2.61E-06	4.65E-06	41.6
1:2	1.70E-06	2.27E-06	3.95E-06	43.2
2:1	1.72E-06	2.83E-06	6.17E-06	27.8
3:1	1.85E-06	3.18E-06	7.21E-06	25.6
1:3	1.84E-06	2.29E-06	3.66E-06	50.2

- Configuration B (with glial sheaths G1a, G1b, G2a, and G2b see figure 1b).
    - Using the same number of total transporters (4600 molecules) used in configuration 1, the transporters were populated in configuration 2.

- Configuration with the transporter molecules distributed in the ratio 4:2:3:1 in glial sheaths G1a, G1b, G2a, and G2b resulted in a P_{syn} that was 12.3 % of P_{ex}.

- Surface areas of glial sheaths G1a, G1b, G2a, and G2b are in the ratio 6 : 11: 14 : 19.

- We observed the following concentration values with various total transporter ratios

Ratio	P_{syn} (μM)	P_{mGluR} (μM)	P_{ex} (μM)	P_{ex}/P_{syn} *100
1:1:1:1	1.06E-06	1.33E-06	6.43E-06	16.52
4:3:2:1	1.12E-06	1.57E-06	9.03E-06	12.39
1:2:3:4	1.25E-06	1.38E-06	4.95E-06	25.37
8:7:3:2	1.12E-06	1.57E-06	9.02E-06	12.40
2:3:7:8	1.25E-06	1.38E-06	4.95E-06	25.33
10:9:8:7	1.06E-06	1.37E-06	7.04E-06	15.01
4:2:3:1	1.12E-06	1.57E-06	9.06E-06	12.36

- A lower concentration at P_{syn} is observed with a total transporter distribution highest on the sheath facing synapse and decreasing as we reach G2b. If the order is reversed we only achieve 50% of value.

- As observed from the table for lower gradients, Glial sheath G1a should be populated with 4/10 of total molecules. If G1a has less than 4/10 of total molecules P_{syn} would be much higher, It is observed that with a

transporter distribution in the ratio 4:3:2:1 is more desirable than the distribution ratio 10:9:8:7 in G1a, G1b, G2a, and G2b.

- Configuration C (with glial sheaths G1a, G1b, G2a, G2b, G3a and G3b)
    - As in configuration A and configuration B same number of total transporter (4600 molecules) are distributed in Configuration C.
    - Surface areas of G1a, G1b, G2a, G2b, G3a and G3b are in the ratio 3 : 5 : 7 : 10 : 11 : 14.

Ratio	P_{syn} (A)	P_{mGluR} (B)	P_{ex} (C)	P_{ex}/P_{syn} *100
1:1:1:1:1:1	8.38E-07	9.80E-07	6.28E-06	13.33
6:5:4:3:2:1	8.45E-07	1.09E-06	9.20E-06	9.19
1:2:3:4:5:6	1.12E-06	1.18E-06	4.75E-06	23.60
6:5:2:1:4:3	7.80E-07	1.01E-06	7.45E-06	10.46
4:3:6:5:2:1	8.69E-07	1.04E-06	8.02E-06	10.83
6:4:5:3:2:1	8.45E-07	1.09E-06	9.20E-06	9.188
12:11:10:9:8:7	8.15E-07	9.91E-07	7.13E-06	11.43

    - The trend seen configuration 2 is observed here as well, the molecules on the inner most sheath facing synapse has highest density. The transporter molecules to be populated in G1a should be greater than 1/6 of total molecules.

- The ratio that achieved lowest synaptic concentration was 6 : 4 : 5 : 3 : 2 : 1 , a similar pattern also yielded same result in configuration B.

RESULTS

CASE I: Keeping Total transporters (moles) constant, and distributing them into different in glial sheaths

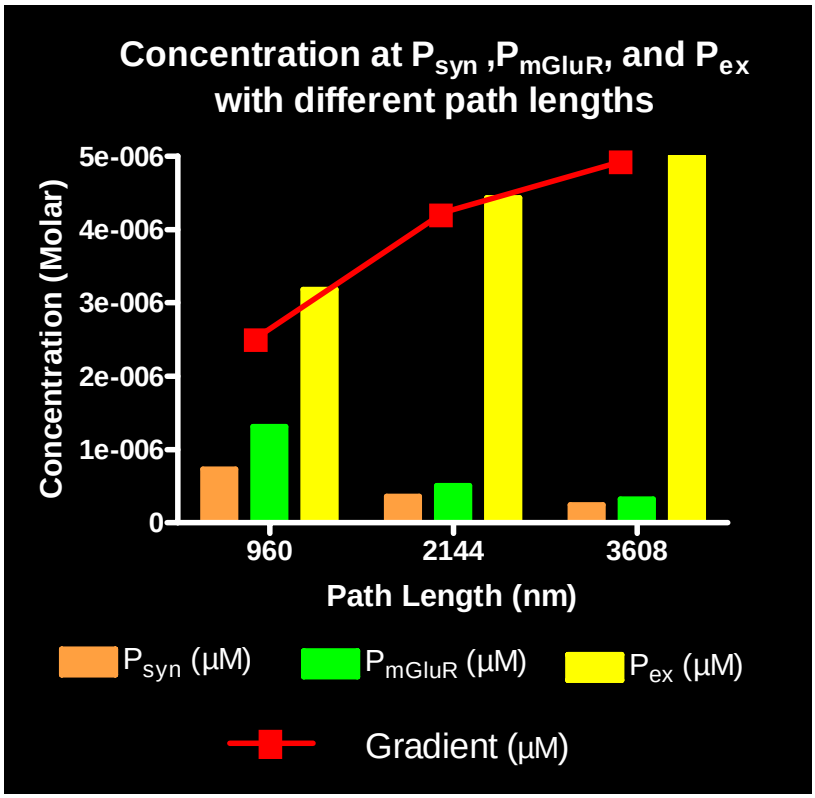

Figure 2 Concentrations observed in synapse, near mGluR and extracellular space for configuration A,B, and C.

Path Length (nm)	P_{syn} (µM)	P_{mGluR} (µM)	P_{ex} (µM)	Gradient(µM)
a) 960	7.31E-07	1.31E-06	3.18E-06	2.45E-06
b) 2144	3.60E-07	5.06E-07	4.43E-06	4.07E-06
c) 3608	2.43E-07	3.21E-07	5.00E-06	4.76E-06

Table 1. Variation of gradient with path length, with constant transporter molecules. A higher gradient is observed in the configuration with distributed low density of transporters. Configuration A with a path length of 960 nm and transporter density twice the higher range could not achieve a gradient more than 2.5 µM. Hence, the transporter distribution is needed in system with low transporter densities and higher extracellular concentrations.

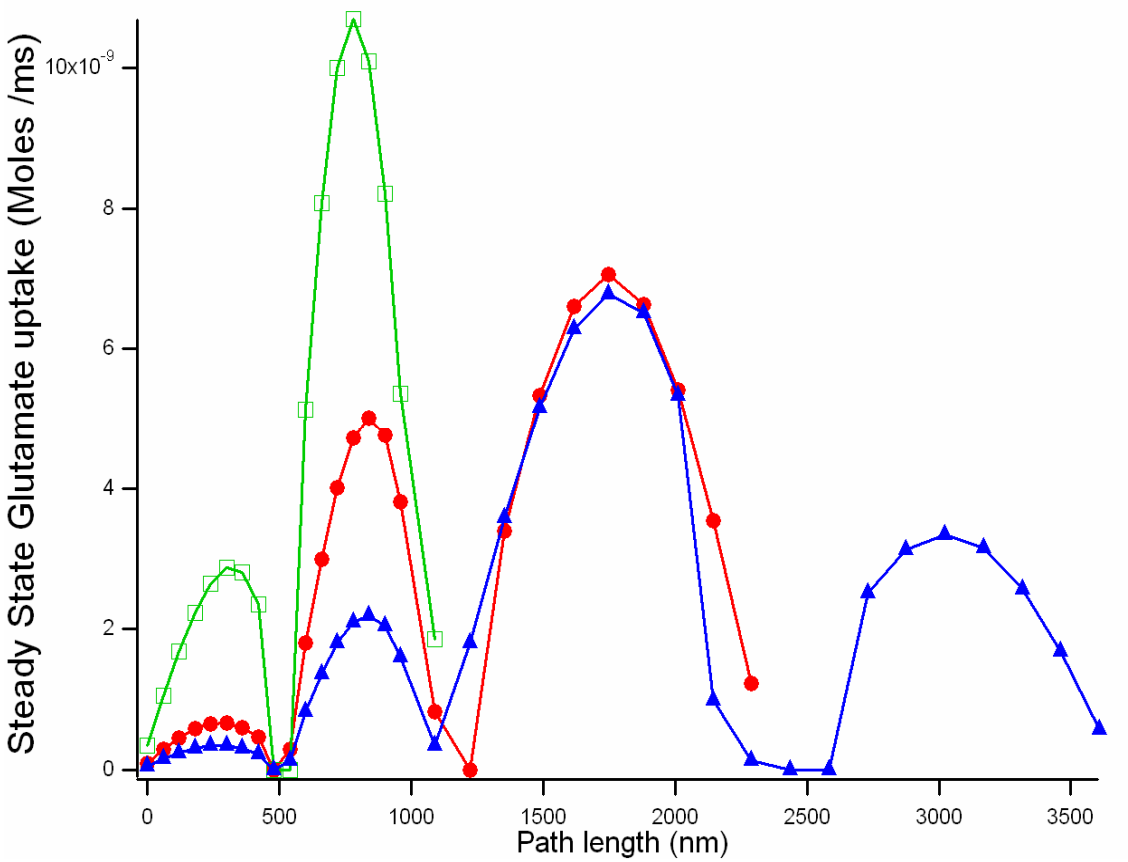

Figure 3 Steady state uptake rates for three configurations **green** (configuration A - 960nm path length) , red (configuration B -2144 nm) and blue (configuration C -3608 nm). At distances 500,1000 and 2500 nm (refer figure 1) concentration is very low since, there are no or very few transporters on the either side of the extracellular gap.

- At steady state the uptake is maximum in sheaths closest to the extracellular space, due to the constant flow of glutamate entering the glia.

- Even though transporter concentration is higher near the synapse the steady state uptake is smaller in all cases.

- With high transporter density and high uptake the configuration with 960 nm path length cannot achieve a gradient to sustain 5 μM in extracellular space.

CASE II: Maximum density of transporters used for all glial sheaths:

- Estimated surface density values for the nucleus accumbens is 22-35% (550-3780 molecules/μm^2) of the value in the hippocampus and cortex. Populating all sheaths with 3780 molecules/ μm^2 (maximum value) and 550 molecules/ μm^2 (minimum value) the concentrations at P_{syn}, $P_{mGluR,}$ and P_{ex} were

	Maximum density of transporters (3780 molecules/μm^2) /sheath			
	P_{syn}	P_{mGluR}	P_{ex}	% age difference between P_{syn} and P_{ex}
Configuration A	1.68E-06	2.27E-06	4.05E-06	58.60
Configuration B	1.06E-07	1.45E-07	2.03E-06	94.78
Configuration C	8.45E-09	1.16E-08	1.15E-06	99.26

	Mimimum density of transporters (550 molecules/μm^2) /sheath			
	P_{syn}	P_{mGluR}	P_{ex}	% age difference between P_{syn} and P_{ex}
Configuration A	2.33E-05	2.40E-05	2.60E-05	10.57
Configuration B	5.73E-06	6.00E-06	1.11E-05	48.42
Configuration C	1.49E-06	1.57E-06	5.55E-06	73.23

- As observed from the table the maximum and minimum gradients (%age P_{ex}-P_{syn}/P_{ex}) achievable by configuration A is 58% and 11% respectively. In configuration B it is 94.7% and 48% respectively. In configuration C the maximum and minimum gradient achievable is 99.26% and 73.23%.

REFERENCES

Bergles DE, Jahr CE (1997) Synaptic activation of glutamate transporters in hippocampal astrocytes. Neuron 19:1297–1308.

Cholet N, Pellerin L, Magistretti PJ, Hamel E (2002) Similar perisynaptic glial localization for Na+, K+-ATPase alpha 2 subunit and the glutamate transorters GLAST and GLT-1 in the somatosensory cortex. Cereb Cortex 12:515-525.

Danbolt NC (2001) Glutamate uptake. Prog Neurobiol 65:1-105

Lehre KP, Danbolt NC (1998) The number of glutamate transporter subtype molecules at glutamatergic synapses: chemical and stereological quantification in young adult rat brain. J Neurosci 18:8751-7.

PUBLICATIONS, CONFERENCES AND OTHER PRESENTATIONS

JOURNAL PAPERS

- **Pendyam,S.**, Mohan,A., Knackstedt,LA., Melendez,R., Kalivas,PW., and Nair,SS., "Computational model of extracellular glutamate in the nucleus accumbens predicts neuroadaptations by chronic cocaine". Journal of Neuroscience (In review).

BOOK CHAPTERS

- Mohan, A., **Pendyam, S.,** Li, G., Gall J., Kalivas, P., and Nair, S.S., "Computational models of neuronal networks – Modeling neuroplasticity in Glu transmission due to cocaine," chapter in *New Research on Neuronal Networks*, Nova Science Publishers, New York (to appear).

IN PREPARATION

- **Pendyam S**, Mohan A, Kalivas PW, and Nair SS, "Glial morphology for a PFC-Nac glutamatergic synapse". *(in preparation).*

CONFERENCE PAPERS AND ABSTRACTS

- **Pendyam S**, Mohan A, Kalivas PW, and Nair SS, "Modeling glutamate homeostasis in PFC-Nac Synapse," *Society for Neuroscience Abstract*, Atlanta, GA, 2006.
- **Pendyam S**, Mohan A, Kalivas PW, and Nair SS, "Computational model of extracellular glutamate in the nucleus accumbens predicts the impact by chronic cocaine," *Presented at the Nano-conference 2007,University of Missouri – Columbia, 2007*.